

THESIS

BIOMECHANICS OF TRANS APICAL MITRAL VALVE IMPLANTATION

Submitted by

Evan Kienholz Koenig

Graduate Degree Program in Bioengineering

In partial fulfillment of the requirements

For the Degree of Master of Science

Colorado State University

Fort Collins, Colorado

Summer 2014

Master's Committee:

Advisor: Lakshmi Prasad Dasi

Ashok Prasad  
Christopher Orton

Copyright by Evan Kienholz Koenig 2014

All Rights Reserved

## ABSTRACT

### BIOMECHANICS OF TRANS APICAL MITRAL VALVE IMPLANTATION

Heart disease is the number one killer in the United States. Within this sector, valve disease plays a very important role: Approximately 6% of the entire population has either prolapse or stenosis of the mitral valve and this percentage only increases when looking only at the elderly population. Transapical mitral valve implantation has promised to be a potential therapy for high-risk patients presenting with MR; however it is unclear what the best method of securing a valve within the mitral annulus may be to provide a safe and efficient valve replacement.

The objective of this research is to study and understand the underlying biomechanics of fixation of transapical mitral valves within the native mitral annulus. Two different transapical mitral valve prosthesis designs were tested: One valve design has a portion of the leaflets atrialized such that it has a shorter stent height and the valve itself sits within the native annulus, the other design is not atrialized and protrudes further into the left ventricle. The valves were implanted in a left heart simulator to assess leaflet kinematics and hemodynamics using high speed imagery and particle image velocimetry techniques. An in vitro passive beating heart model was then used to assess the two different fixation methods (namely, anchored at the apex vs. anchored at the annulus) with respect to paravalvular regurgitation. Leaflet kinematics and hemodynamics revealed proper leaflet coaptation and acceptable pressure gradients and inflow fillings; however, both designs yielded elevated turbulence stresses within

the ventricle. At 60 beats per minute, leaflet opening and closing times were both under 0.1 seconds, max Reynolds shear stresses were between 40 and 60 N/m<sup>2</sup> and maximum velocities were approximately 1.4 m/s. Assessment of the different fixation methods during implantation revealed the superiority of the atrialized valve when anchored at the annulus ( $p < 0.05$ ), but showed no such comparison during tethered implantation. In addition to the results of statistical testing, observations show that the importance of the relationship between ventricular stent height and fixation method compared with native anatomy plays an important role in overall prosthesis function regardless of implantation method.

# TABLE OF CONTENTS

TABLE OF CONTENTS .....	iv
1.1 Aims and Hypotheses .....	3
1.1.1 Aim 1 .....	3
1.1.2 Aim 2 .....	3
1.2 Organization.....	4
2.1 The Heart.....	5
2.2 The Mitral Valve .....	5
2.2.1 Anatomy and Mechanics .....	5
2.2.2 Valve Disease.....	10
2.3 Heart Valve Interventions.....	11
2.3.1 Treatment of Valve Disease.....	11
2.3.2 Minimally Invasive Interventions .....	12
2.3.3 Transcatheter Aortic Valve Implantation .....	13
2.3.4 Minimally Invasive Mitral Repair .....	15
2.3.5 Trans Apical Mitral Valve Implantation (TAMI).....	15
2.3.6 Current Trans Apical Mitral Implantation Research .....	17
2.4 Hemodynamics in Prosthetic Valves.....	23
3.1 Chapter Introduction.....	26

3.2 Materials and Methods.....	26
3.2.1 Valves.....	26
3.2.2 Left Heart Simulator.....	28
3.2.3 GOA Calculation.....	31
3.2.4 Particle Image Velocimetry.....	33
3.2.5 Flow Conditions.....	34
3.2.6 Statistical Analysis.....	35
3.3 Results and Discussion.....	35
3.3.1 Flow and Pressure.....	35
3.3.2 GOA and leaflet kinematics.....	37
3.3.3 Flow and Turbulence.....	39
4.1 Chapter Introduction.....	45
4.2 Aim 2 Methods.....	46
4.2.1 In Vitro Beating Heart Simulator.....	46
4.2.2 DAQ and Control.....	50
4.2.3 Heart Preparation.....	51
4.2.4 Valve Implantation.....	54
4.2.5 Data Measurements and Calculations.....	56
4.2.6 Statistical Analysis.....	60
4.3 Results and Discussion.....	60

4.5 Potential Future Work .....	71
5.1 Aim 1 – Summary .....	73
5.2 Aim 1 - Limitations .....	74
5.2.1 Idealized Left Ventricle .....	74
5.2.2 Non Blood Analogue as Working Fluid .....	74
5.2 Aim 2 – Summary .....	75
5.4 Aim 2 – Limitations.....	76
5.4.1 Paradoxical Ventricular Motion .....	76
5.4.2 Porcine Model as Human Analogue .....	77
5.4.3 Replicating In Vivo Valve Implantation.....	77
5.4.4 Flow Probe Error.....	78
Appendix I .....	84
Appendix II .....	86
Data from IVBHS Experimentation .....	86
Appendix III .....	98

## LIST OF TABLES

Table 1. The resulting maximum Reynolds Shear Stress (RSS) for each valve under a range of heart rates. Each valve and heart rate was tested at a cardiac output of 5 liters per minute. Also shown is the maximum velocity for each take from the ensemble averaged velocity field.....	40
Table 2. Detailed information regarding flow probes and pressures sensors used during IVBHS experimentation.....	50
Table 3. Tabular results from In Vitro Beating Heart Simulator (IVBHS) experiments. The two different annulus measurements are displayed as well as the resulting mitral regurgitant fraction for each heart under each valve condition. The annular measurement is the maximum measured for each measurement.....	64
Table 4. Results from IVBHS experiments after correcting for the viscosity difference between the working fluid and blood.....	64
Table 5. Raw data for the geometric orifice area calculations of each valve design.....	85

## LIST OF FIGURES

Figure 1. The anatomical relationship of the primary components of the mitral valve: mitral valve leaflets, chordae tendinae and the papillary muscles. ....	6
Figure 2. The geometry of the mitral leaflets as well as the labeling convention for the varying regions of the leaflets can be seen above [3].....	7
Figure 3. Illustrates the dynamics and three dimensionality of the mitral annulus between systole (B, D) and diastole (A, C). A and B are normal functioning mitral valves. C and D show the altered dynamics of the mitral annulus with Myxomatous Degeneration. Myxomatous Degeneration refers to a pathological weakening of the body's connective tissue [5]. ....	8
Figure 4. The complex hierarchy of the chordae tendinae and their anatomical positioning between the papillary muscles and mitral valve leaflets [4]. ....	9
Figure 5. Comparison of minimally invasive interventions and the conventional open heart approach. A and B show transfemoral and transapical approaches respectively while C is a conventional open heart surgery (Edwards Lifesciences). ....	13
Figure 6. Two examples of TAVI valves. The Medtronic Corevalve can be seen on the left and the Edwards Sapien can be seen on the right. ....	14
Figure 7. Abbott Laboratories has developed Mitraclip, a percutaneous method to implement an edge-to-edge mitral repair technique (Abbott Laboratories).....	15
Figure 8. Double crowned stent designed by Ma and colleagues[30] .....	17

Figure 9. Ventricular (top) and atrial (bottom) views of the prosthesis developed by a collaboration between the University of Wisconsin School of medicine and the University Hospital Schleswig-Holstein [29]. ..... 19

Figure 10. Tissue ingrowth of the atrial element of this prosthesis seen several months post implantation [26] ..... 20

Figure 11. The “D” shape of the Tiara is evident as well as the fibrous tissue growth on the atrial skirt. View is from the left atrium of a sacrificed pig [33]. ..... 21

Figure 12. Stentless valve developed by Gillespie and colleagues. Relies on ventricular hooks for both ventricular and atrial fixation. The atrial fixation method is unique to this valve, as the others discussed have utilized an atrial skirt or cuff [34] .... 23

Figure 13. Valve implanted by Gillespie and colleagues. Shows the implanted valve from the atrial side (A) and the ventricular side (B) [34]. ..... 23

Figure 14. Both valve designs used during all experiments. On the right is the non-atrialized design and on the left is the atrialized design. The atrialized portion of the leaflets of the atrialized design can be seen in the lower left of the image. .... 27

Figure 15. Valve orientation in the idealized left ventricular block. The aortic valve is position above the mitral valve. In this picture a mechanical tilting disc valve is in the aortic position with the atrialized valve design in the mitral position. .... 28

Figure 16. Schematic of the Left Heart Simulator (LHS). ..... 29

Figure 17. A 21mm Medtronic Hancock tissue valve was used in the aortic position of the idealized left ventricular during all experimentation (Medtronic Inc.). ..... 30

Figure 18. LabVIEW VI built to control the Left Heart Simulator (LHS). User input fields include heart rate and stroke volume as seen above. The acquire data button and output data file path can also be seen..... 31

Figure 19. The process of going from a raw high speed image (A) to a shell (D) that can be used to geometric orifice area (GOA) of the valve during its open phase. ImageJ and the plugin SIOX were used to process all images. .... 32

Figure 20. Raw high speed image (A) and resulting vector field (B) from PIV experimentation..... 34

Figure 21. Pressure and flow wave forms for each valve design at a heart rate of 60 beats per minute and cardiac output of 5 liters per minute ..... 36

Figure 22. Pressure and flow wave forms for each valve design at a heart rate of 120 beats per minute and cardiac output of 5 liters per minute ..... 37

Figure 23. High speed imaging reveals proper coaptation for both the atrialized design (A) and the non-atrialized design (B)..... 38

Figure 24. Computational vector fields resulting from the fluid flow through a healthy mitral valve during diastole [37]..... 39

Figure 25. Vorticity dynamics for each valve at a heart rate of 60 bpm and cardiac output of 5 lpm. The vectors represent velocity and the contours represent opposite directions of out of plane vorticity. The atrialized valve design is on the left and the non-atrialized design is on the right. .... 41

Figure 26. Vorticity dynamics for each valve at a heart rate of 120 bpm and cardiac output of 5 lpm. The vectors represent velocity and the contours represent opposite

directions of out of plane vorticity. The atrialized valve design is on the left and the non-atrialized design is on the right..... 42

Figure 27. Vector fields with contours representing Reynolds shear stress ( $N/m^2$ ) throughout diastole for a heart rate of 60bpm and cardiac output of 5lpm. Atrialized valve design is on the left and the non-atrialized design is on the right. Images go in sequence from the beginning of diastole (top) to the end of diastole (bottom). ..... 43

Figure 28. Vector fields with contours representing Reynolds shear stress ( $N/m^2$ ) throughout diastole for a heart rate of 120bpm and cardiac output of 5lpm. Atrialized valve design is on the left and the non-atrialized design is on the right. Images go in sequence from the beginning of diastole (top) to the end of diastole (bottom). ..... 44

Figure 29. Schematic of the In Vito Beating Heart Simulator (IVBHS). ..... 47

Figure 30. LabVIEW VI built to control the In Vitro Beating Heart Simulator (IVBHS). User input fields include heart rate and duty cycle as seen above. The VI also includes a data acquisition toggle button as well as graphical displays of the following:  
 Ventricular Pressure, Aortic Pressure, and Flow Rate. .... 51

Figure 31. Porcine heart as received from the abattoir, before extraneous tissue has been removed. .... 52

Figure 32. Fully prepared porcine heart for use in the IVBHS. Ventricular port is seen on the right while the aortic port is seen on the top of the heart. .... 53

Figure 33. The orientation and attachment points of the tethers on the larger profile stent valve. The attachment points are look identical on the valve design that contains more atrialized leaflets. .... 55

Figure 34. Each valve design implanted as viewed from the left atrium. A) Larger stent profile design with the larger atrial cuff. B) Atrialized stent design with smaller cuff. .... 56

Figure 35. An example of a mitral sizing tool used by surgeons. The tool can be used to measure the intercommissural distance (A), the total area of the valve (B) and the septo-lateral distance (C) [38]. ..... 57

Figure 36. Flow profiles and illustration of area under the curve for aortic flow probe (A) and total flow probe (B). In (A) the blue area minus the red area results in the standard stroke volume while the blue area in (B) corresponds to the total forward stroke. .... 59

Figure 37. A column plot of the resulting mitral regurgitant fraction (MRF) for each heart and valve condition..... 61

Figure 38. A column plot of the mitral regurgitant fraction (MRF) for each heart and condition after the viscosity correction has been completed. .... 61

Figure 39. A box plot representing the viscosity corrected MRF values for each valve condition. NA represents the non-atrialized valve design and A represents the atrialized valve design. The native condition was left out because there is not a suitable viscosity correction for the condition. .... 62

Figure 40. Cartoon of atrialized vs. non-atrialized suture implantation. Due to the large stent height of the non-atrialized design, the atrial cuff does not secure properly to the atrial floor. .... 65

Figure 41. LVOT obstruction shown during systole (A) and diastole (B). In both images the White arrow indicates the aortic valve and the Red arrow indicates the direction of the aorta. The valve stent can be seen in contact with the inner wall of the left ventricle. .... 66

Figure 42. An occurrence of the native leaflets interfering with bioprosthesis function as captured by Doppler imaging. The closed leaflets of the bioprosthesis are pointed out by 'A' and the closed leaflets of the native mitral valve are indicated by 'B.' In this view, the open area that would be the left atrium can be seen at the top of the image and the valves open into the left ventricle which would be below the image. .... 67

Figure 43. An illustration of interference by the native mitral leaflets. The top image shows both valves during diastole and the bottom image shows the valves during systole. If the leaflets are long enough, they wrap around the top of the stent of the valve and begin to cover the orifice. .... 68

Figure 44. Poor atrial fixation of the non-atrialized valve design implanted in the sutured fashion. (A) shows a gap forming between the atrial skirt of the valve and the atrial floor (pointed out by the white arrow) during high pressure systole and (B) shows that same gap disappearing during diastole. .... 71

## Chapter 1: Introduction

Heart disease is the leading cause of death in the United States, causing nearly 1 in every 4 deaths (CDC, 2010). Within heart disease there are many subcategories of diseases that affect the heart, these include: coronary artery disease, valve disease, congenital heart defects and many others. Valve disease is one category that places a large burden on the medical system. It is estimated that 2.5% of the population of the United States have been diagnosed with valve disease and the prevalence of mitral valve disease is nearly double that of aortic valve disease (AHA, 2014). Treatment of aortic valve diseases has seen the development of percutaneous valve replacements (transcatheter aortic valve implantation, TAVI), but this technology has not yet made its way to mitral valve replacements yet. Given the high prevalence of mitral valve disease and the increasingly elderly patient population that presents with this disease, there is a great need for minimally invasive mitral valve therapies. Several percutaneous repair strategies have been developed with the Mitraclip device being one of the most successful on the clinical stage. The device is designed to result in a mitral repair based on the Alfieri edge-to-edge technique and has reported the results of clinical trials [1]; however, due to the complexity of the anatomy of atrio-ventricular valves, percutaneous mitral valve replacement has yet to see clinical trials.

Preclinical animal studies of various trans-apical mitral valve implantation (TAMI) valve prototypes have seen some success; with several seeing first-in-man implantations. However, no studies (animal or in vitro) have been undertaken to truly understand the biomechanics of various methods of fixing TAMI valves within the mitral annulus.

Valves implanted within the mitral annulus cannot rely on radial force to anchor them as seen in their aortic counterparts. For this reason, valves must contain a method to secure them on both the atrial and ventricular sides of the atrioventricular junction. Typically, an atrial skirt is used that hugs the atrial floor and prevents the valve from migrating into the left ventricle. On the ventricular side, there are two prominent means of fixation: Tethering and hooking. Tethered implantation mimics the native chords and uses a series of tethers attached to the valve stent that are then anchored at the apex of the heart to prevent valve migration. The other method of implantation, hooking, uses a series of hooks that grasp onto the native valve tissue. The hooks typically grab onto a combination of mitral valve leaflet and chordae tendinae to keep the valve in place. There are many factors that must be considered when picking a certain fixation method: ventricular remodeling, myocardial dynamics, varying anatomy between patients, ease of orientation and deployment, and many others.

While a benchtop model can only begin to approach answering the question for some of these considerations, it is a start that can hone the focus when moving on to animal studies. In addition, animal studies are both very costly and very time-consuming. Studying newly developed prosthetic valves in an accurate in-vitro simulator can result in a quicker pipeline to clinical trials and application to patients.

It is the aim of this research to apply engineering principles to the documentation of the biomechanics of varying ventricular fixation methods of TAMI valves and their related effect on paravalvular leakage.

This study will begin with standard study of the hemodynamics and mechanics of several TAMI valves in an ideal left heart simulator and move to an in-vitro beating heart simulator utilizing porcine hearts to assess varying fixation methods and they're effects on mitral valve competence.

## 1.1 Aims and Hypotheses

### 1.1.1 Aim 1

Aim 1: Evaluate leaflet kinematics and flow through each of two valve designs using a left heart simulator and Particle Image Velocimetry (PIV)

Hypothesis 1: Valve mechanics and hemodynamics will results in flows that adequately resemble physiologic conditions

A left heart simulator will be used to test each of two valve designs. The left heart simulator utilizes a clear, acrylic block to simulate a left ventricle and house the valves. This clear block allow for high speed imaging of the valve leaflets to assess leaflet kinematics and also allows for particle image velocimetry (PIV) to be performed to assess the fluid mechanics through the valves. The data gathered from performing PIV will be used to determine vorticity, maximum velocities, and Reynolds shear stresses.

### 1.1.2 Aim 2

Aim 2: Evaluate and understand the difference in mechanics between two different methods of ventricular fixation for transapical mitral valves.

Hypothesis 2: Due to the variability of native mitral valve tissue, tethering will prove be a superior option for ventricular fixation.

An in-vitro beating heart simulator will be used to artificially create a beating heart using pressurized fluid and a porcine heart. Two different transapical mitral valve designs will be implanted in two different fashions each: tethered and sutured. The resulting paravalvular regurgitation in each of the conditions will be measured using multiple flow probes. Pressure taps and cardiac Doppler imaging will also be used to assess valve function.

## 1.2 Organization

Chapter 2 will contain a literature review of information pertaining to this research. Following this will be a chapter for each of the Aims of this research. Each chapter will contain both the methodology and results for each aim. The methodologies used in each aim are vastly different and thus do not appear in a single methods chapter. In the chapter for each aim, the results and discussion will also occur simultaneously in a single section. Following these chapters will be a summary of the findings as well as a discussion of the limitations for each aim.

## Chapter 2: Literature Review

### 2.1 The Heart

The heart is a muscular organ that generates the force necessary to deliver blood to the entire body. The heart consists of four separate chambers: two upper chambers known as atria and two lower chambers known as ventricles. The ventricles are the chambers that work to deliver blood through both the pulmonary and systemic circuits. The heart can be subdivided into two distinct sides: the right side receives blood from the systemic circuit and sends blood to the lungs to be oxygenated while the left side receives oxygenated blood from the pulmonary circuit and sends it to the rest of the body. The left side has to generate a significantly greater amount of force to deliver blood to the entire systemic circuit and thus occupies a much larger portion of the heart and contains a much thicker myocardium [2].

There are four valves found in the heart: the pulmonary valve, aortic valve, tricuspid valve and mitral valve. The two former exist at the beginning of major arteries leaving the heart (pulmonary artery and the aorta) while the two later exist in the atrioventricular junction: The tricuspid valve sits between the right atrium and the right ventricle and the mitral valve sits between the left atrium and the left ventricle.

### 2.2 The Mitral Valve

#### 2.2.1 Anatomy and Mechanics

Proper mechanics of the mitral valve (MV) are the result of a complex interaction between four components whose main goal is to prevent the backflow of blood from the

left ventricle into the left atrium during systole, but allowing such flow during diastole. These four components are the annulus, leaflets, chordae tendinae and papillary muscles. Figure 1 illustrates the anatomic relationship of each of these four components.

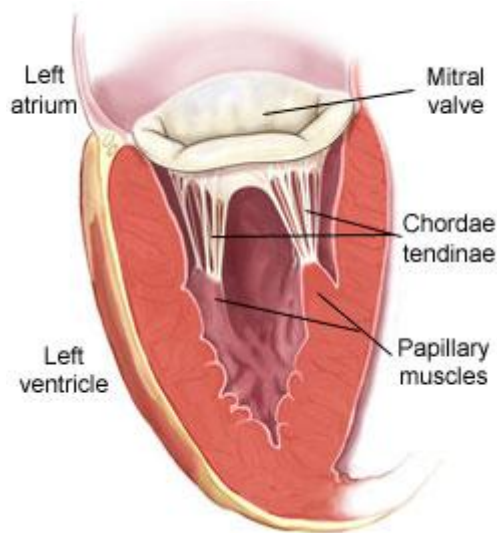


**Figure 1. The anatomical relationship of the primary components of the mitral valve: mitral valve leaflets, chordae tendinae and the papillary muscles.**

In the MV it is that valve leaflets that are ultimately responsible for preventing regurgitant blood flow. The MV is a bileaflet valve consisting of the anterior (aortic) and posterior (mural) leaflets. The leaflets are asymmetric in shape, but have nearly identical surface areas. Both of the leaflets are part of a continuous band of tissue anchored to the mitral annulus at the base and to the chordae tendinae at their free edge. They are indented at two points and these indentations are known as commissures. The

commissures divide this continuous band of tissue into two distinct leaflets for proper opening during diastole and they also aid in proper leaflet coaptation during systole [3]. In adults, the posterior leaflet has indentations that typically divide the leaflet into three scallops, or segments, along the free edge: These scallops are labeled as P1, P2 and P3. The anterior leaflet also has similar labeling, however, it is arbitrarily segmented as A1, A2, and A3 corresponding to the adjacent posterior leaflet scallop [4]. These designations can be seen in Figure 2. The leaflet designations are also important landmarks when measuring the septo-lateral (anteroposterior diameter) of the mitral

annulus. This diameter is the annulus diameter measured from the center of A2 to the center of P2. The beginning and end points of this measurement are where the leaflets integrate with the mitral annulus. The second important annulus diameter is the commissure-commissure diameter. This measurement is as the name implies, the distance between the two commissures.

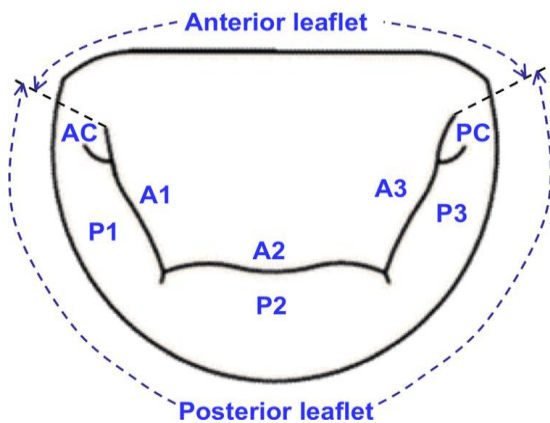


**Figure 2. The geometry of the mitral leaflets as well as the labeling convention for the varying regions of the leaflets can be seen above [3].**

Although the mitral annulus is what physically separates the left atrium from the left ventricle, it is not visible from the atrium as it is deeper and roughly 2mm external to the visible hinge of the leaflets [3]. The annulus itself takes what is known as a 'D' shape and is conventionally divided into both posterior and anterior portions. The anterior

portion contains the anterior leaflet and is also anatomically coupled to the aortic annulus. The posterior portion encompasses the rest (larger portion) of the mitral annulus and is composed of fibrous tissue periodically interrupted by fat. The discontinuous nature of the fibrous tissue is thought to be why the posterior annulus experiences more enlargement than the anterior [5]. Enlargement of the mitral annulus is of great consequence on the performance of the MV.

The mitral annulus is uniquely situated very near to myocardial fibers of the heart. This causes the geometry of the mitral annulus to change throughout the cardiac cycle. During systole, the area of the mitral annulus is asymmetrically reduced and takes the shape of a three dimensional saddle. This reduces the area that the mitral leaflets must

cover and increases the leaflet area available for proper coaptation [3]. This motion that the annulus undergoes is known as annular folding and is theorized to be caused by several mechanisms. During ventricular contraction, the entire mitral annulus is translated apically; however, due to the inconsistent anatomical composition of the annulus, the anterior and posterior portions translate differently. This results in a folding of the annulus along the intercommissural axis [5]. These dynamics and three dimensionality are illustrated in Figure 3. This figure also shows the altered annular motion and shape associated with a common degenerative disease affecting the mitral

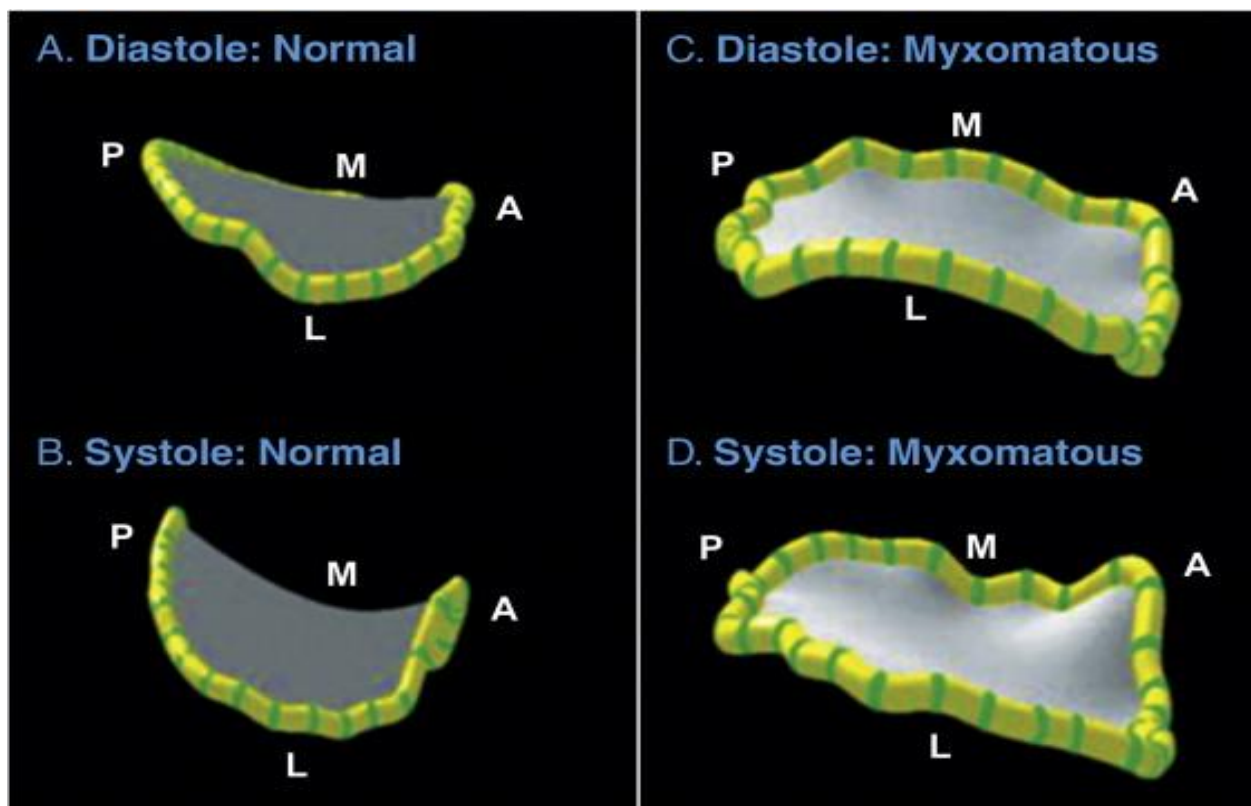


**Figure 3.** Illustrates the dynamics and three dimensionality of the mitral annulus between systole (B, D) and diastole (A, C). A and B are normal functioning mitral valves. C and D show the altered dynamics of the mitral annulus with Myxomatous Degeneration. Myxomatous Degeneration refers to a pathological weakening of the body's connective tissue [5].

valve, myxomatous degeneration. Myxomatous degeneration refers to a weakening of the body's connective tissue is often associated with a prolapsed mitral valve.

The chordae tendinae (CT) and papillary muscles (PM) act as a suspension system for the mitral valve. They facilitate leaflet opening during diastole and prevent the leaflets from migrating toward the left atrium during systole. The CT primarily attach the mitral valve leaflets to a PM imbedded in the ventricular wall, however, in some cases the CT attach directly to the ventricular wall. There is a hierarchy of CT structure and function with a variety of sizes, shapes and bifurcations. A dissected example of the CT, PM complex can be seen in Figure 4.

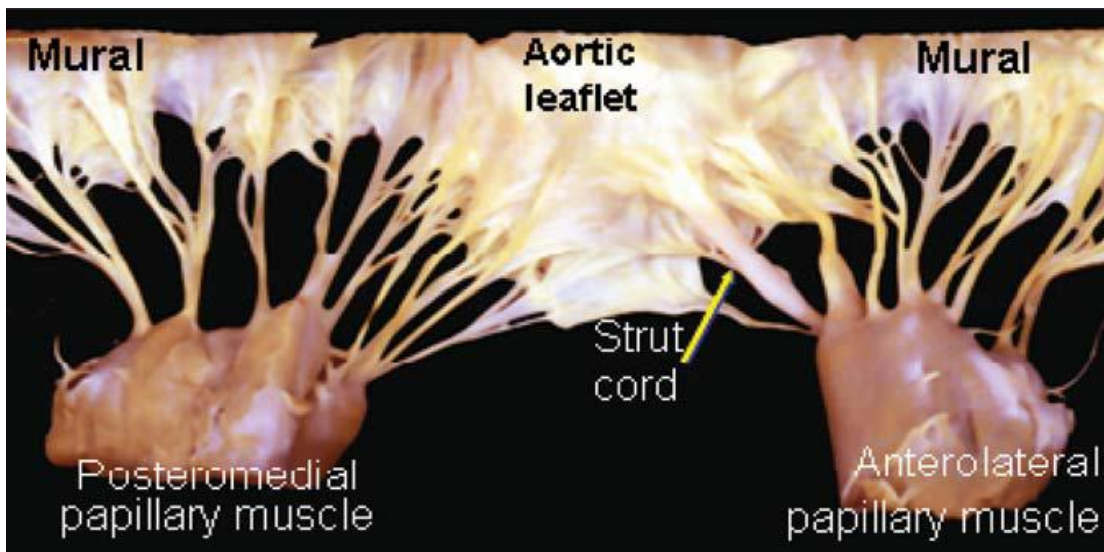


**Figure 4. The complex hierarchy of the chordae tendinae and their anatomical positioning between the papillary muscles and mitral valve leaflets [4].**

The PMs function to adjust tension on the CT throughout the cardiac cycle. There are typically two groups of papillary muscles attached to the ventricular wall. The naming convention is based on their position relative to the two mitral leaflet commissures: anterolateral and posteromedial. It has been shown that papillary muscles maintain

their distance from the mitral annulus throughout the entire cardiac cycle: Thus, contracting during systole and elongating during diastole. From this observation, it has been hypothesized that the papillary muscle, chordae tendinae complex act as shock absorbers that maintain the geometric shape of the mitral valve throughout the cardiac cycle [6].

### 2.2.2 Valve Disease

The mitral valve is arguably the most complex of all the valves in the human heart and is also happens to be the most commonly diseased. Typical mitral valve conditions are stenosis, regurgitation, and leaflet prolapse; ranking in order of commonality with stenosis being the least prevalent and leaflet prolapsed being the most prevalent. Its estimated that up to 5% of the population presents with mitral leaflet prolapsed, while 1% experience mitral stenosis [7].

Stenosis, or obstruction of the mitral valve, can have several causes. One of these causes is rheumatic fever; however, the availability of antibiotics in developed countries has all be eradicated this cause, but it is important to note that this is still relatively common disease in developing countries. Another more common cause of mitral stenosis is calcified valve leaflets often seen in elderly patients. Stenosis leads to an insufficient amount of blood flow during diastole causes a larger portion of blood to remain in the left atrium. This can result in left atrium stretch and resulting blockage of the cardiac electrical pathways which leads to irregular heartbeats and resulting palpitations [7].

Mitral regurgitation (MR), or valve leakage, occurs when the mitral valve does not close completely during systole (contraction of the left ventricle). When this occurs, blood returns into the left atrium instead of proceeding to systemic circulation. Causes of MR are divided into two different categories: organic and functional. Organic MR occurs when there is a problem with the mitral valve apparatus itself that results in MR. Organic MR can further be broken down into rheumatic (resulting from rheumatic fever) and degenerative MR. Degenerative MR primarily presents itself as a prolapse of one or both of the mitral valve leaflets. Functional MR occurs when regurgitation is secondary to a disease of the left ventricle. Functional MR is typically caused either by ischemia or some other cause of dilation of the left ventricle. The enlargement of the left ventricle can either result in a stretching of the mitral annulus or excessive tethering forces being placed on the chordate tendinae, both of which lead to poor leaflet coaptation.

## 2.3 Heart Valve Interventions

### 2.3.1 Treatment of Valve Disease

A faulty mitral valve can be treated with one of two methods: replacing the faulty valve or repairing it. There exist many different repair options for mitral valves including, but not limited to: leaflet resection, balloon valvuloplasty, annuloplasty ring implantation, edge-to-edge repair and neo-chordae implant. There also exist nearly as many options for valve replacement. An abundance of companies produce commercially available and FDA and CE approved mitral valve prostheses. Since the first implanted heart valve in 1952, upwards of 50 different heart valve designs have been developed and in 2009 nearly three million have been implanted worldwide [8].

Although there is some debate as to which method of mitral valve treatment is superior, several studies have recently shown the non-inferiority of mitral valve replacement as a treatment. A recent, randomized study by the NIH reported severe ischemic MR patient outcomes between valve repair and replacement: Patients were randomized between valve annuloplasty and valve repair. After a 24 month follow up, there were no health outcomes between groups; the only significant difference was a 32.6% chance of recurrent MR in the repair group versus 3.2% in the replacement group; although this recurrent MR did not lead to any noticeable health problems in the repair group over the course of the study [9].

A significant portion of the patient population that experiences mitral regurgitation is elderly: The American Heart Association reports that of all patients aged 75 and above, 10% present with some form of mitral regurgitation [10]. Many patients – especially these elderly patients previously mentioned – present with significant co morbidities or left ventricular dysfunction that is severe enough such that they are not referred for conventional surgical treatment [11]. Because of this large patient population that is unable to go through conventional open heart surgery, it is becoming more and more important to develop minimally invasive interventions for MR.

### 2.3.2 Minimally Invasive Interventions

The large draw for minimally invasive interventions is the reduced surgical trauma experienced by the patient. This reduced trauma results in a significantly reduced recovery time as well as a much lower peri-operative risk. This reduced risk is a necessity for high-risk patients to be eligible for the therapy. Figure 5 shows the comparative invasiveness of open heart surgery compared to two minimally invasive

options. The two images on the left show a transfemoral and transapical insertion respectively with the image on the right being a standard open heart procedure. During a transfemoral implantation, a catheter based delivery system is used to deliver the prosthesis to the heart via the femoral artery. Transapical implants use a small incision to access the apex of the heart and deliver the prosthesis.

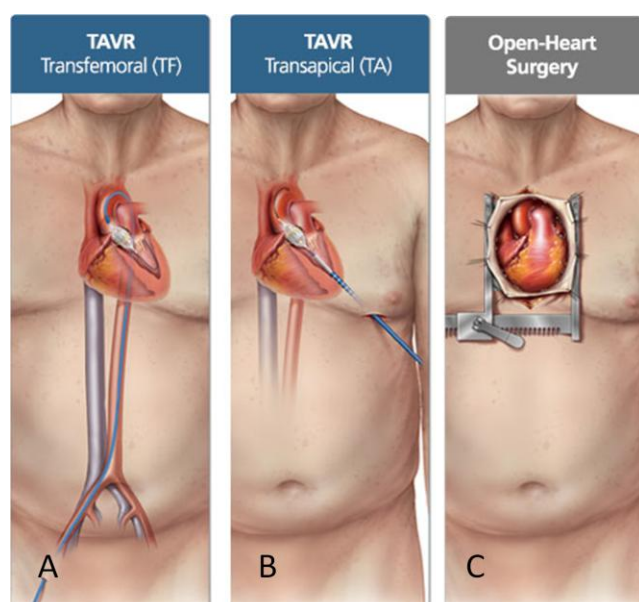


**Figure 5. Comparison of minimally invasive interventions and the conventional open heart approach. A and B show transfemoral and transapical approaches respectively while C is a conventional open heart surgery (Edwards Lifesciences).**

In a study looking at patients with severe aortic stenosis, more than 30% of the patients were deemed ineligible for conventional aortic valve replacement surgery because of multiple co-morbidities [12].

Though this statistic focuses on inoperable patients with aortic valve disease, a similar analogue can be seen in the mitral valve: As quoted previously, of all patients 75 and above, 10% present with present

with MR [10]. With this increase in age comes an increase in co-morbidities and high surgical risk, which results in many of these patients not being recommended for conventional mitral valve replacement.

### 2.3.3 Transcatheter Aortic Valve Implantation

Although not suitable for native mitral valve dysfunction, the first trans-catheter aortic valve implantation (TAVI) was introduced in 2002. Since initial approvals in Europe in

2007, a significant number of inoperable patients have undergone a TAVI procedure (estimates from 2011 put that number at greater than 20,000). There are currently two commercially available TAVI valves in the United States: Edwards Sapien and Medtronic Corevalve [13]. These valves – seen in Figure 6– are typically implanted via the femoral artery or apex of the heart and either balloon expanded or self expanded into the native aortic valve. Clinical results of TAVI show much promise, with most results showing increased long term outcomes of patients receiving this procedure [14, 15].



**Figure 6. Two examples of TAVI valves. The Medtronic Corevalve can be seen on the left and the Edwards Sapien can be seen on the right.**

TAVI valves are designed to utilize their radial force to maintain their position within the very cylindrical aortic root. Given the lack of uniformity within the native mitral annulus, these valves are not suitable for implantation in the mitral position; however, there has been some clinical success with implanting these TAVI valves within failing bioprosthesis in the mitral position [16-18]. In addition, there have been several reported cases of TAVI valve-in-annuloplasty ring implantations [18-20]. Although there has been some success in expanding the potential for TAVI implantation, there have

been relatively few minimally invasive interventions developed with the mitral valve apparatus as the primary target [17].

#### 2.3.4 Minimally Invasive Mitral Repair

In recent years, several percutaneous mitral repair technologies have emerged and are at various levels of development. These percutaneous technologies include: edge-to-edge repair, annuloplasty, and chordal implant. One of the select few of these technologies, Mitraclip – a percutaneous intervention based on the Alfieri technique, seen in Figure 7– has presented the results of a randomized clinical trial and thus far appears to be a reasonable option for a select group of patients [11]. In practice, however, the Mitraclip implantation has been a very difficult procedure requiring a very experienced medical team.



**Figure 7. Abbott Laboratories has developed Mitraclip, a percutaneous method to implement an edge-to-edge mitral repair technique (Abbott Laboratories).**

#### 2.3.5 Trans Apical Mitral Valve Implantation (TAMI)

In addition to these repair technologies, several research groups have begun pre-clinical animal studies of minimally invasive mitral valve replacements; to date, there have also been two in man implantations of TAMI valves. Compared to TAVI procedures, the mitral valve apparatus presents a much more complicated geometry

and approach. Firstly, it has been shown that leaving the native mitral apparatus intact is important in retaining proper left ventricular geometry and function [21]. This means that mitral implant design must take into account the native anatomy of the mitral apparatus and leave it as undisturbed as possible. Also, due to the asymmetry, lack of rigidity and dynamics of the native mitral annulus; TAMI valves cannot rely on radial force for secure attachment within the native mitral annulus as has been seen in aortic and pulmonary valve replacements. Any attempt at using radial force to anchor the prosthesis can have deleterious effects: obstruction of the left ventricular outflow tract (LVOT), systolic anterior motion (SAM), valve migration into either the left atrium or left ventricle, distortion of the native annulus and its dynamics, compression of the adjacent coronary circumflex artery, and impingement of the conducting systems of the heart [22, 23].

There have been several solutions proposed for valve fixation without using radial force. Two different options appear to be the most common among valves undergoing pre clinical trials: tethering the valve to the apex of the heart as seen in the native mitral apparatus and hooking onto the native mitral valve tissue (chordae tendinae and native leaflets) to anchor the valve in place [22-29].

The first experimental study in the field of minimally invasive atrioventricular valve replacement was published in 2004 [30]. Since this first publication, several more research groups have published their own animal studies on their own uniquely developed valve devices. To date, two in-man implantations of minimally invasive mitral bioprosthesis have occurred. First in man was claimed by CardiAQ Valve Technologies, Inc. in June of 2012 as a compassionate treatment for an elderly man

experiencing severe MR. The second implantation was conducted using the Tiara mitral valve developed by Neovasc, Inc. The implant – occurring in January of 2014 – was uneventful and no adverse events were reported at least two months post op. Although Neovasc Inc. has published preclinical animal studies, CardiAQ Valve Technologies has released no results of any of their preclinical studies. In addition to CardiAQ, there are several other minimally invasive mitral prostheses being developed privately; thus the status of their development nor any preclinical results can be discussed in any length.

In the following section, the valve design and preclinical results for all published research will be discussed.

### 2.3.6 Current Trans Apical Mitral Implantation Research

In 2004 Liang Ma and colleagues implanted a double crowned design in adult swine



**Figure 8. Double crowned stent designed by Ma and colleagues[30]**

[30]. In this publication, the surgeon implanted the valves via an incision in the left atrium instead of the apex of the heart.

An image of the valve used by Ma et al can be seen in Figure

8. The native annulus sits in between the two nitinol ‘crowns’

in the stent body in order to prevent valve migration. The

animals survived no more than 3 hours post implantation;

postmortem evaluation was conducted to confirm that the

native annulus was in between the two ‘crowns’ of the stent body. Three of the eight

swine implanted showed mild paravalvular leakage (PVL), but it was determined that

the source of this was annulus, prosthesis size mismatch: The native annulus was, in

each case, at least 20% larger than the stent size. No fracture of the valve stent was observed; however valve migration into the left ventricle occurred in one animal, which resulted in complete LVOT obstruction. The study was proof that valve implant in this position was feasible with further studies expected to test if the implantation will also be feasible in humans.

In 2005, Boudjemline et al implanted a percutaneous tricuspid valve replacement [31]. The geometry of the tricuspid valve varies from the MV; however, due to the atrioventricular position; the tricuspid valve contains the same complexities associated with percutaneous implantation of a mitral valve. The valve design used was similar to that reported by Ma and involved a tubular section flanked on both sides by a disc like structure. One each of these discs was to be deployed into the right atrium and right ventricle of the sheep in order to prevent valve migration and ensure proper sealing of the stent body. Boudjemline et al replaced the tricuspid valve in 8 ewes (4 in a chronic study and 4 in an acute study) with moderate success. Of the four animals implanted acutely, one had maldeployment with the ventricular disc becoming ensnared in the native chordae of the right ventricle. In the chronic portion of the study, three of the four animals possessed good hemodynamics and no sign of leakage during the 1 month follow up period. The fourth of these animals had a stent fracture which resulted in a PTFE tear and subsequent severe paravalvular leakage.

Between 2008 and 2011 collaboration between the University of Wisconsin School of Medicine and the University Hospital Schleswig-Holstein has produced a series animal studies documenting their trials of various TAMI valves. An example of an early design

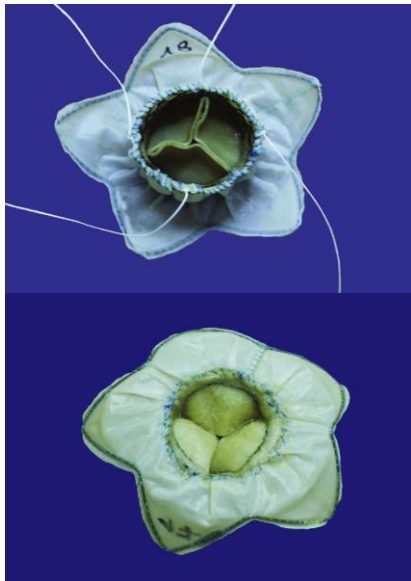


**Figure 9. Ventricular (top) and atrial (bottom) views of the prosthesis developed by a collaboration between the University of Wisconsin School of medicine and the University Hospital Schleswig-Holstein [29].**

can be seen in Figure 9. This design utilizes an atrial skirt as the atrial fixation method and, contrary to the previous publications, a tethered design for ventricular fixation. The tethers are designed to be attached to the ventricular wall to prevent migration into the atrium during systole. All iterations of these valves have resulted in no LVOT obstruction as well as no systolic anterior motion (SAM) cause by displacement of the native mitral valve tissue. Early acute implantation studies by this group resulted in no to mild paravalvular leakage and no stent migration up to one hour post implantation [23, 29]. Later publications implanted and observed similar valves until animal death. Early

animal deaths (less than one week) were reported to be primarily the result of atrial stent mal-deployment, while late death (greater than one week) were mostly attributed to stent fixation failure: Either fracture of the atrial springs or failure of the ventricular fixation device [22, 25, 27]. A more long term study was completed with follow ups for the animals reaching 2 months post implantation. Again, the one early animal death noted was due to maldeployment of the atrial portion of the stent. Only mild or trace MR was observed in the remaining animals with no valve migration; however two pigs were

reported to have fracture of the atrial springs, but this fracture did not appear to affect the performance of the valve. Tissue ingrowth of the atrial element of the valve was seen to be 50% at 1 month post implantation and 70% at two months post implantation [26]. This tissue ingrowth can be seen in Figure 10. The effects of this tissue in growth were not elaborated on further. This valve has shown to create a successful seal with easily reproducible valve deployment.

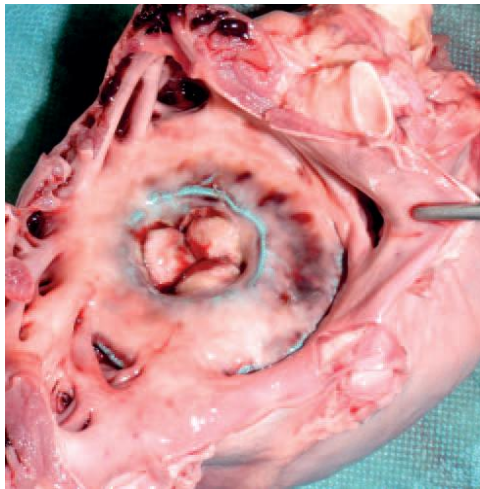


**Figure 10. Tissue ingrowth of the atrial element of this prosthesis seen several months post implantation [26]**

The Tiara valve developed by Neovasc Inc. has published both acute and long term pre-clinical trials and has recently become the second transapical mitral valve to be implanted in man [32]. The Tiara has taken into account the ‘D’ shaped geometry of the native mitral valve. As seen in Figure 11 the valve possess a ‘D’ shape, mirroring the native mitral annulus. Similar to previous valves, the Tiara uses an atrial skirt to fix

the atrial side of the tent, but it utilizes a unique method of ventricular fixation. The Tiara relies on a set of hooks that grasp the native mitral leaflets and hold the valve stent in place.

In the acute ovine model, implantation was performed on 36 sheep. Implantation was successful in 29 of these animals; however, both the valve itself and the surgical

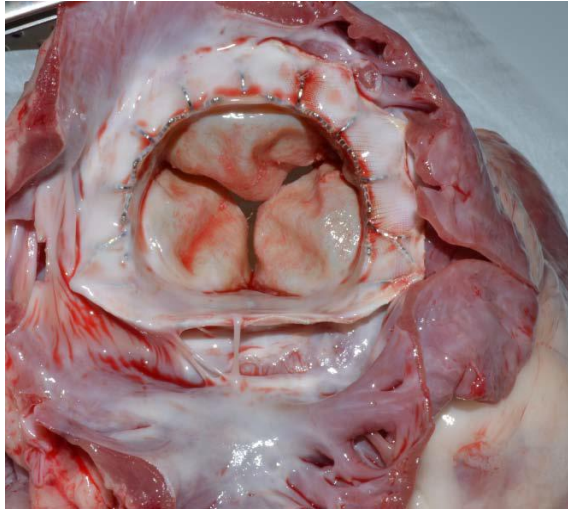


**Figure 11. The “D” shape of the Tiara is evident as well as the fibrous tissue growth on the atrial skirt. View is from the left atrium of a sacrificed pig [33].**

methods were being perfected during the time period. The unsuccessful cases were due to improper valve position (n=3), failure of ventricular fixation hooks to properly engage (n=2) and ventricular fibrillation (n=2). None of the successfully implanted animals showed any LVOT obstruction and only animals with a significant mismatch between the annulus and valve size showed significant PVL. In the acute model, the animals were monitored for a maximum of 96 hours before they were sacrificed.

In the chronic model, seven sheep were implanted and monitored for approximately 150 days. All 7 animals were clinically stable and showed normal behavior throughout the entire follow-up period. Two animals showed a mild degree of valvular MR and six animals had mild to moderate PVL. None of the animals were shown to have LVOT obstruction and the left ventricle maintained normal size and function. A view from the left atrium in the sacrificed pigs show that there is substantial fibrous tissue growth on the atrial skirt of the Tiara valve. There was also a thin layer of growth along the ventricular surface of the valve as well. The tissue growth on the atrial element can be seen in Figure 11. A cadaveric study resulted in proper geometric positioning of the

valve as well as proper engagement of both anchoring systems in all 24 hearts studied. These 24 hearts included both healthy and diseased hearts: Of the diseased hearts, twelve had moderate to severe MR and 7 had congestive heart failure.

In 2013 Gillespie and colleagues implanted a prototype transcatheter mitral valve in ten sheep in an acute ovine study [34]. An image of the prototype valve used in this study can be seen in Figure 12. Contrary to what has been seen in the other studies, this valve utilizes an atrial hook system to grasp the supra-annular tissue and create a seal. The ventricular fixation mechanisms is similar to that seen in the Tiara valve. This valve; however, utilizes a significantly greater number of hooks to grasp the native valve leaflets and chordae tendinae. Details in the publication are scarce; however it appears that implantation was successful with no LVOT obstruction or paravalvular leakage reported. It is important to note that the authors believed this to be merely a proof of concept for the valve and thus performed implantation utilizing cardiopulmonary bypass on the sheep. The surgeons arrested the heart and performed the implantation through the left atrium. While this isn't the same implantation methodology seen by other publications, the authors believe that it was adequate for a first proof of concept paper. An image of the implanted valve from both atrial and ventricular vantage points can be seen in Figure 13.

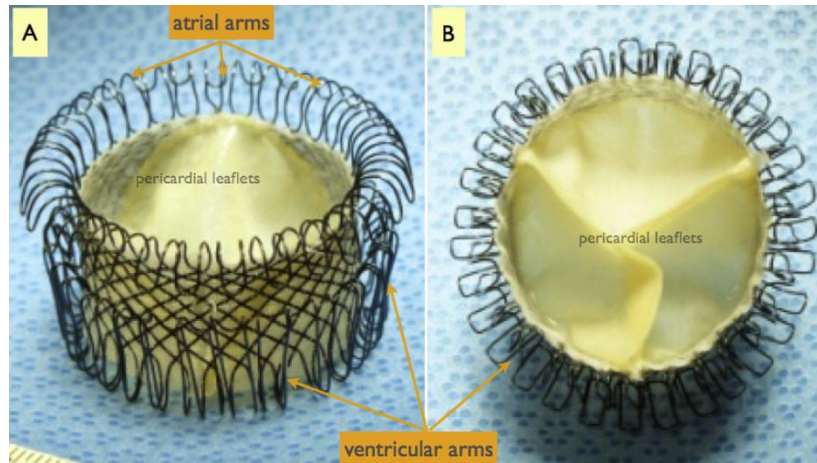


**Figure 12. Stentless valve developed by Gillespie and colleagues. Relies on ventricular hooks for both ventricular and atrial fixation. The atrial fixation method is unique to this valve, as the others discussed have utilized an atrial skirt or cuff [34]**

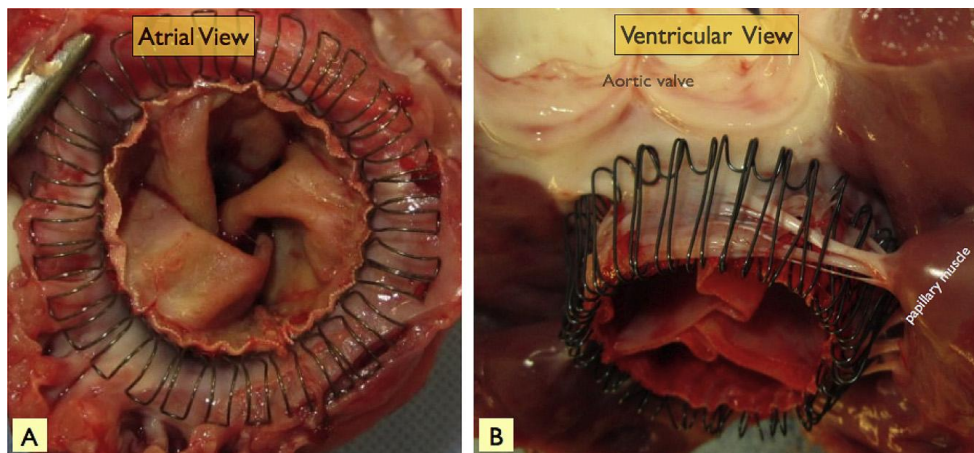


**Figure 13. Valve implanted by Gillespie and colleagues. Shows the implanted valve from the atrial side (A) and the ventricular side (B) [34].**

## 2.4 Hemodynamics in Prosthetic Valves

The anti-coagulation therapy is needed to prevent thrombotic events in the patient.

These events have two causes of significant in this study: shear stress induced damage to red blood cells (RBCs) or contact with the material of the prosthesis. Since bioprosthetic valves are the focus of this study, the second cause may be ignored:

Bioprosthetic valves are constructed from biological tissue that should present no

immune response when implanted. Thus, the focus is on shear induced damage to the blood components.

Elevated levels of shear stress around the implanted valve have been shown to cause potential lethal damage to RBCs and potential activation of platelets. These can lead to thrombus formation or a thromboembolic event, both of which have the potential to be fatal. It has been shown that Reynolds shear stress (RSS) is a primary contributing factor to the total shear stress experienced by these blood elements. It has been theorized that RSS is not indicative of the actual mechanical environment experienced by blood elements [35]; however, turbulent shear stress patterns in the vicinity of the prosthetic valve have also been said to be indicative of long term clinical efficacy [36] and turbulence levels are a required measure to be investigated, as seen in the international standard ISO 5840 for cardiovascular implants.

Reynolds shear stress is the component of total stress that accounts for the fluctuation of momentum due to turbulence in fluid flow.  $RSS, \tau$ , can be mathematically represented by

$$\tau = \rho \overline{u'v'},$$

where  $u'$  and  $v'$  are the velocity fluctuations in the x and y direction respectively, where x can be considered the axial direction and y considered the transverse direction.

The turbulence within a series of related velocity fields, and thus the RSS values, can be calculated by ensemble averaging multiple cardiac cycles under the same flow conditions. Reynolds stresses can be thought of as the variation of a velocity field from

the ensemble averaged velocity field. These velocity, and thus, momentum fluctuations are the cause of RSS.

## Chapter 3: Aim 1 - LHS Simulator and PIV

### 3.1 Chapter Introduction

Aim 1 is to assess the leaflet kinematics and flow through each of two different mitral valve prosthesis designs. Particle Image Velocimetry will be used to map the flow through each valve at a variety of flow conditions. These data can then be used to perform turbulence analysis, among other things, to determine the turbulence stresses that the flow experiences. This stress has been determined to be a significant cause of blood and platelet damage after prosthetic valve implantation [35].

Another measure of valve performance is the geometric orifice area of the valve. This is a measure of the maximal orifice area through which the working fluid travels during peak flow. This measure will be calculated using high speed imaging in conjunction with image analysis software.

### 3.2 Materials and Methods

#### 3.2.1 Valves

The valves used in experimentation are an iteration of Avalon Medical's Mitraseal canine mitral valve replacement. This valve is currently in clinical trials and is being developed in conjunction with Dr. Orton at the Colorado State University Veterinary Hospital. Images of these valves can be seen in Figure 14. By design, the valves are implanted via a trans-apical approach and rely on an atrial cuff and ventricular tethers as fixation methods to keep their place in the mitral annulus. The valves consist of a woven, self-expanding nitinol stent with fixed porcine pericardial leaflets sewn into the

stent tube. Also sewn to the atrial cuff is waterproof membrane to prevent leakage.

The atrialized design (seen on the left in Figure 14) has a stent body diameter of 24mm, a cuff diameter of 39.5mm and a total height of 20.5mm. The non-atrialized design (seen on the right in Figure 14) has a stent body diameter of 24mm, a cuff diameter of 46mm and a total height of 22mm.

The atrialized design features a portion of the leaflets that have been atrialized which results in the valve of the prosthesis sitting directly inside of the native mitral annulus.

This splits the total height of the valve stent between the left atrium and left ventricle.

This valve design is thought to minimize LVOT obstruction and results in fewer areas for



stagnation and subsequent thrombosis formation. The non-atrialized design does not feature atrialized leaflets, instead the actual valve of the prosthesis is well below the native annulus and sits within the left ventricle. These features can all be seen in the figure containing images of the valves.

**Figure 14. Both valve designs used during all experiments. On the right is the non-atrialized design and on the left is the atrialized design. The atrialized portion of the leaflets of the atrialized design can be seen in the lower left of the image.**

### 3.2.2 Left Heart Simulator

The left heart simulator (LHS) is a flow loop that has been fabricated in house in order to simulate the left ventricle of the heart. The LHS consists of the following main

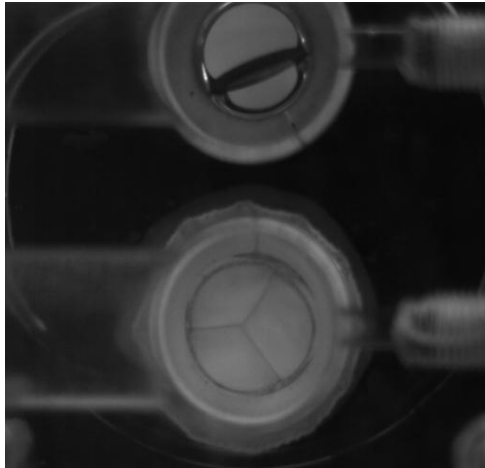


**Figure 15. Valve orientation in the idealized left ventricular block. The aortic valve is position above the mitral valve. In this picture a mechanical tilting disc valve is in the aortic position with the atrialized valve design in the mitral position.**

components: fluid reservoir, acrylic block housing the aortic and mitral valves, linear actuator, compliance chamber, and resistance valve. A schematic of this flow loop can be seen in Figure 16 and a close up of the valve orientation in the idealized left ventricle can be seen in Figure 15. As this flow loop was

designed to simulate the left ventricle of the heart, most of the components of the loop have an analogue in the native heart. The fluid reservoir and acrylic block are the left atrium and

left ventricle respectively with the linear actuator simulating the contraction of the left ventricle.

The linear actuator operates based on input from a custom made LabVIEW VI in order to drive flow through the system. Upon rearward motion of the actuator, water is pulled from the reservoir, through the mitral valve and into the idealized left ventricle (acrylic block). With forward motion of the actuator, water is pushed through the aortic valve, into the compliance chamber, through the resistance valve and back into the fluid reservoir.

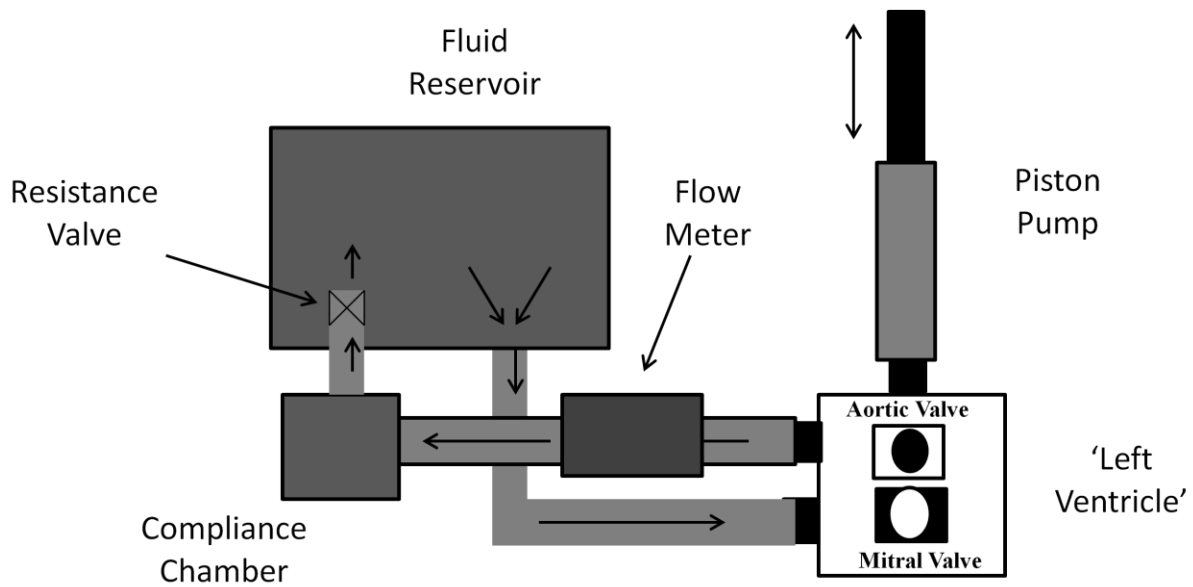


**Figure 16. Schematic of the Left Heart Simulator (LHS).**

The compliance chamber in the LHS is an acrylic cylindrical chamber that receives fluid from the flow probe at its inlet and its outlet leads to the resistance valve. The cylinder is sealed except for two taps at its top; one of these taps leads to a pressure gauge and the other to a bulb pump. Compliance in the system is modulated by adjusting the amount of air in the compliance chamber: The greater the amount of air in the chamber, the greater the compliance.

The resistance valve is a simple ball valve that can be finely modulated to alter the amount of flow able to go through the system. This valve is used in conjunction with the compliance chamber to attain proper physiologic pressure waveforms.

During all experiments a 21mm Medtronic Hancock valve (seen in Figure 17) was used in the aortic position of the left ventricle block.

### 3.2.2.1 Data Acquisition and Control

The LHS is controlled via a LabVIEW VI made specifically for this purpose. The VI allows the user to control the flow conditions of the LHS while reading data from 3 pressure transducers and a flow probe. The pressure transducers measured correspond to the following physiologic measurements: Atrial Pressure, Ventricular Pressure and Aortic Pressure. The flow probe is placed downstream of the aortic valve in order to measure flow through the aortic valve, and thus the cardiac output (CO) of the system.



**Figure 17. A 21mm Medtronic Hancock tissue valve was used in the aortic position of the idealized left ventricular during all experimentation (Medtronic Inc.).**

The raw output of pressure and flow measurements is recorded in units of voltage. Each of the probes was calibrated and then a C++ code is used to process the LabVIEW output and calculate pressures in units of mmHg and flow in mL/second. This code also reports relevant cardiac measures such as mean arterial pressure (MAP), regurgitant fraction (RF), cardiac output (CO) and effective orifice area (EOA).

The linear actuator motion was based on a sine wave function. The VI allows the user to adjust both the frequency and amplitude of this sine wave: Altering these characteristics corresponds to a change in heart rate (HR) and stroke volume (SV) respectively. The HR and SV along with modulating the resistance valve and amount of compliance can be used to attain the proper flow and pressure curves needed by the user. The VI also allows for data collection of each of the three

pressure sensors and the flow probe simultaneously. A screenshot of the VI can be seen in Figure 18.

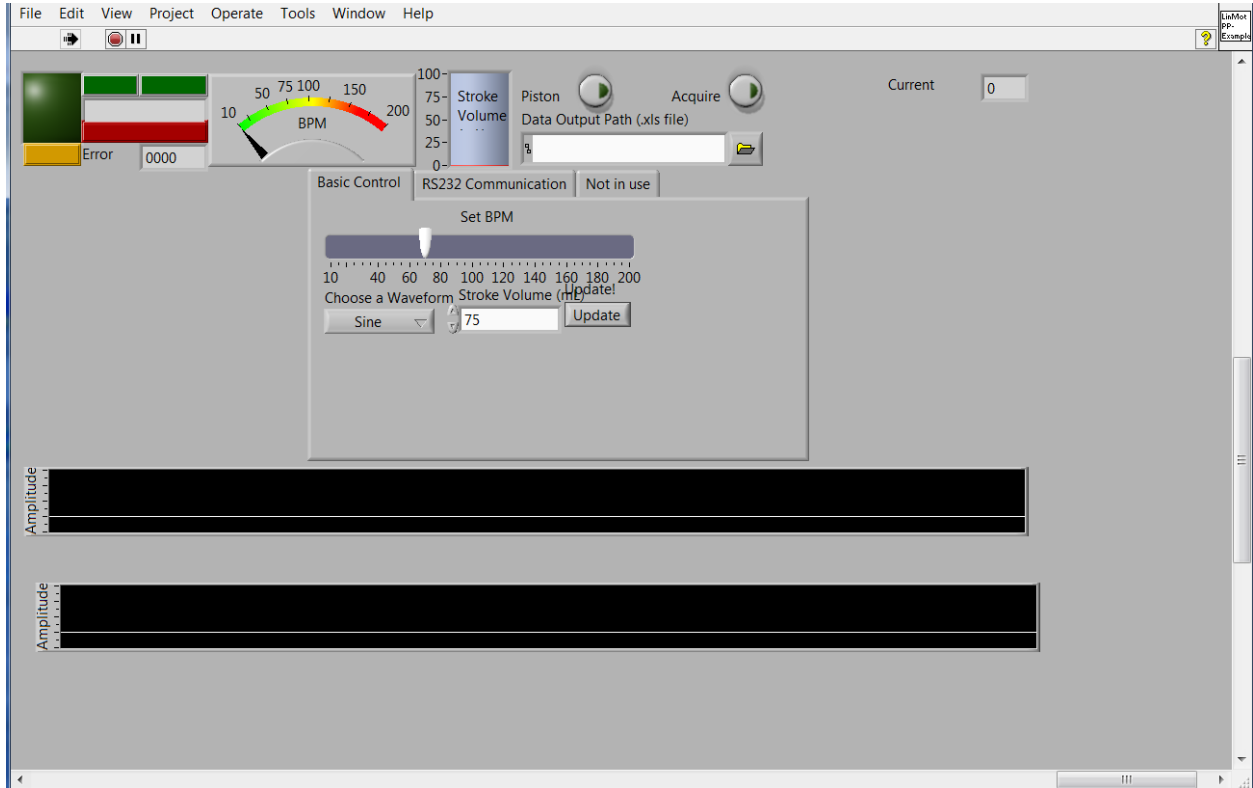


**Figure 18. LabVIEW VI built to control the Left Heart Simulator (LHS). User input fields include heart rate and stroke volume as seen above. The acquire data button and output data file path can also be seen.**

### 3.2.3 GOA Calculation

Unfortunately, the pressure sensors used in the LHS lack the sensitivity needed to determine an accurate pressure gradient across the mitral valve during diastole. For this reason, it was determined to perform GOA analysis as an alternative to EOA measurements.

Each valve was implanted in the LHS and experienced the following conditions: a HR of 60 bpm and a CO of 5 lpm. High speed imaging was captured using at 250 frames per second for each valve design using a high speed camera (Photron, San Diego, CA,

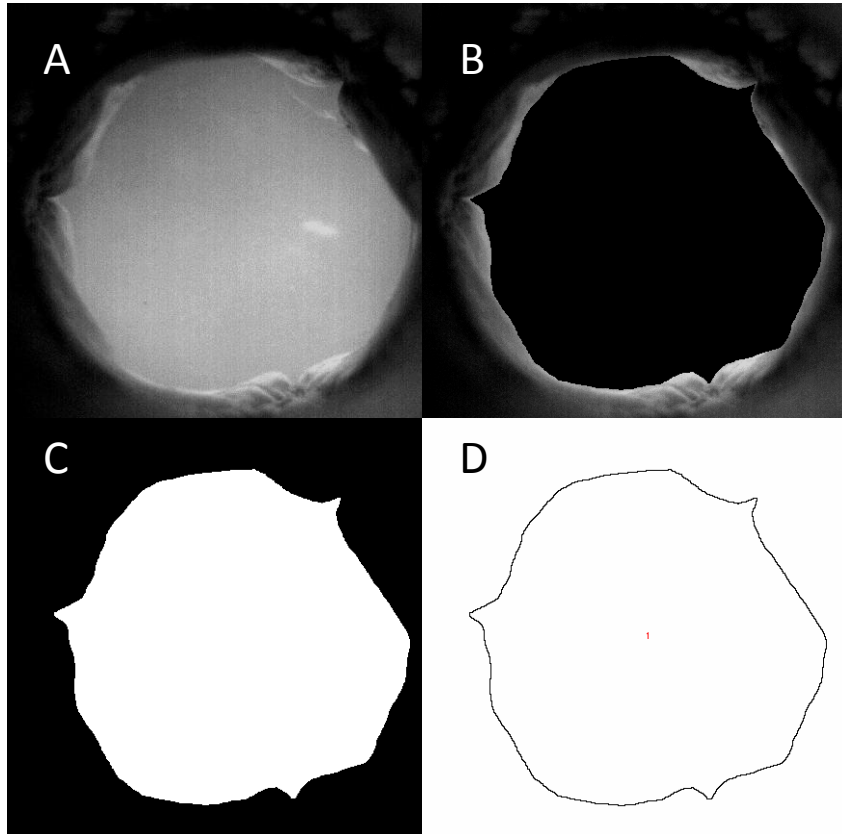


**Figure 19. The process of going from a raw high speed image (A) to a shell (D) that can be used to geometric orifice area (GOA) of the valve during its open phase. ImageJ and the plugin SIOX were used to process all images.**

Model: FASTCAM SA3). Using image J and the SIOX (Simple Interactive Object Extraction) plugin, the geometric orifice area (GOA) for each valve was extracted during peak diastole, GOA measurements were taken for 9 separate frames; this process was then repeated over three separate

cardiac cycles. For each frame in question, contrast was adjusted to produce a distinct boundary at the leaflet edge. In this adjusted image, the boundary of the leaflet was traced to produce a mask of the valve orifice. The SIOX plugin was then used to extract this mask and resulting surface area measured using imageJ. A series of images outlining each of these steps can be seen in Figure 19, the figure progress from A being the raw image to D being the final mask from which the area can be calculated. The mean and standard deviations were then calculated for all measurements taken for each valve design.

### 3.2.4 Particle Image Velocimetry

Particle image velocimetry (PIV) is an unobtrusive, indirect way to measure kinematics within fluid flow. PIV analysis utilizes a combination of micro particle seeded fluid, high speed camera and high powered laser to visualize flow.

The PIV system used was constructed by LaVision Inc. A diode-pump Q-switched Nd:YLF laser (Photonics Industries, Bohemia, NY) was utilized to cast a thin laser sheet and a mirror was used to reflect this laser sheet to centrally transect each the valve through the idealized left ventricular block. Raw images were captured using a high-speed camera synchronized to the laser pulses (Photron, San Diego, CA, Model: FASTCAM SA3). Double frame images were captured at a frequency of 1 kHz. The double pulse laser action is used to illuminate seed particles twice within a very short time period to detect fluid flow with a higher resolution, in these experiments; the double pulse was sent 300 $\mu$ s apart. The fluid was seeded with polyamide particles (Dantec Dynamic Inc.) with a mean diameter of 20 $\mu$ m.

Velocity field data computation was done using LaVision's DaVis flowmaster software and uses a 2D cross-correlation algorithm to identify shifting patterns between frames, resulting in a displacement vector. Each frame is subdivided into small regions termed "interrogation windows." The DaVis software uses 2D cross-correlation to identify the corresponding interrogation windows between frames. This process is what results in the displacement vector. Along with the displacement vector and the time known between frames, it is possible to produce a velocity vector for each window. This process is expanded to each entire frame, and the result is a vector field for each frame.

Raw images captured with the high speed camera and resulting vector field can be seen in Figure 20

From this velocity field data, a custom made MatLab code was created to perform statistical turbulence analysis on each testing condition. This code performed ensemble averaging on 50 cardiac cycles captured under the same flow conditions. From this ensemble averaged vector field, the turbulent fluctuations can be extracted and thus the RSS values are also extracted. The flow velocities can also be extracted from the averaged vector fields. The MatLab code used to perform this operation can be seen in Appendix III.

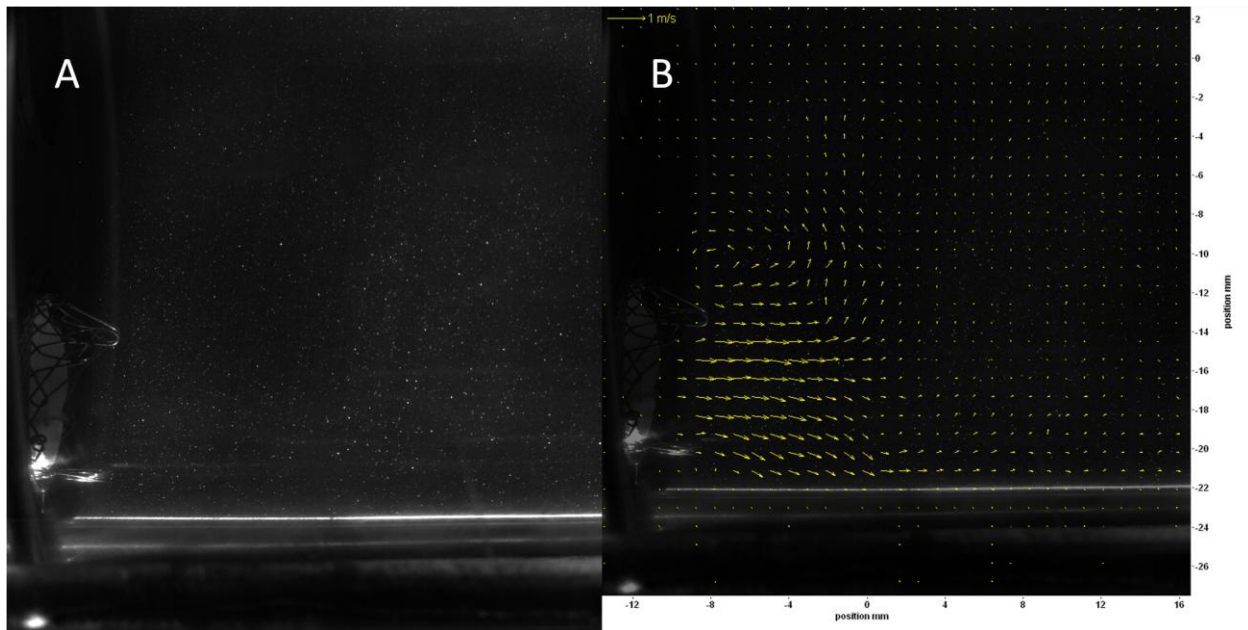


**Figure 20. Raw high speed image (A) and resulting vector field (B) from PIV experimentation.**

### 3.2.5 Flow Conditions

Each valve (Non-atrialized design and atrialized design) were tested at a variety of conditions. Each was tested at three different heart rates: 60 bpm, 90 bpm and 120

bpm. During all of these testing, the cardiac output was maintained at 5 liters per minute.

### 3.2.6 Statistical Analysis

For these methods students t test was used to test statistical significant. Measurements are reported as the mean  $\pm$  one standard deviation.

## 3.3 Results and Discussion

### 3.3.1 Flow and Pressure

Pressure and flow curves for each valve at 60 bpm and 5 lpm can be seen in Figure 21. Peak flow during diastole for this condition was roughly 290 mL/s for the atrialized design and 245 mL/s for the non-atrialized design. Average pressure gradient across the mitral valve during diastole was roughly 4 mmHg for the atrialized design and 3 mmHg for the non-atrialized design.

Pressure and flow curves for each valve at 120 bpm and 5 lpm can be seen in Figure 22. Peak flow during diastole for this condition was roughly 340 mL/s for the atrialized design and 330 mL/s for the non-atrialized design. Average pressure gradient across the mitral valve during diastole was roughly 6 mmHg for the atrialized design and 5 mmHg for the non-atrialized design.

The values of pressure drop across the prosthesis during diastole during these experiments were on the high end of acceptable. In all likelihood, the valves perform acceptably, the pressure taps used in the LHS were not sensitive enough to calculate an accurate EOA value and thus it is believed that the pressure drop readings are also artificially high.

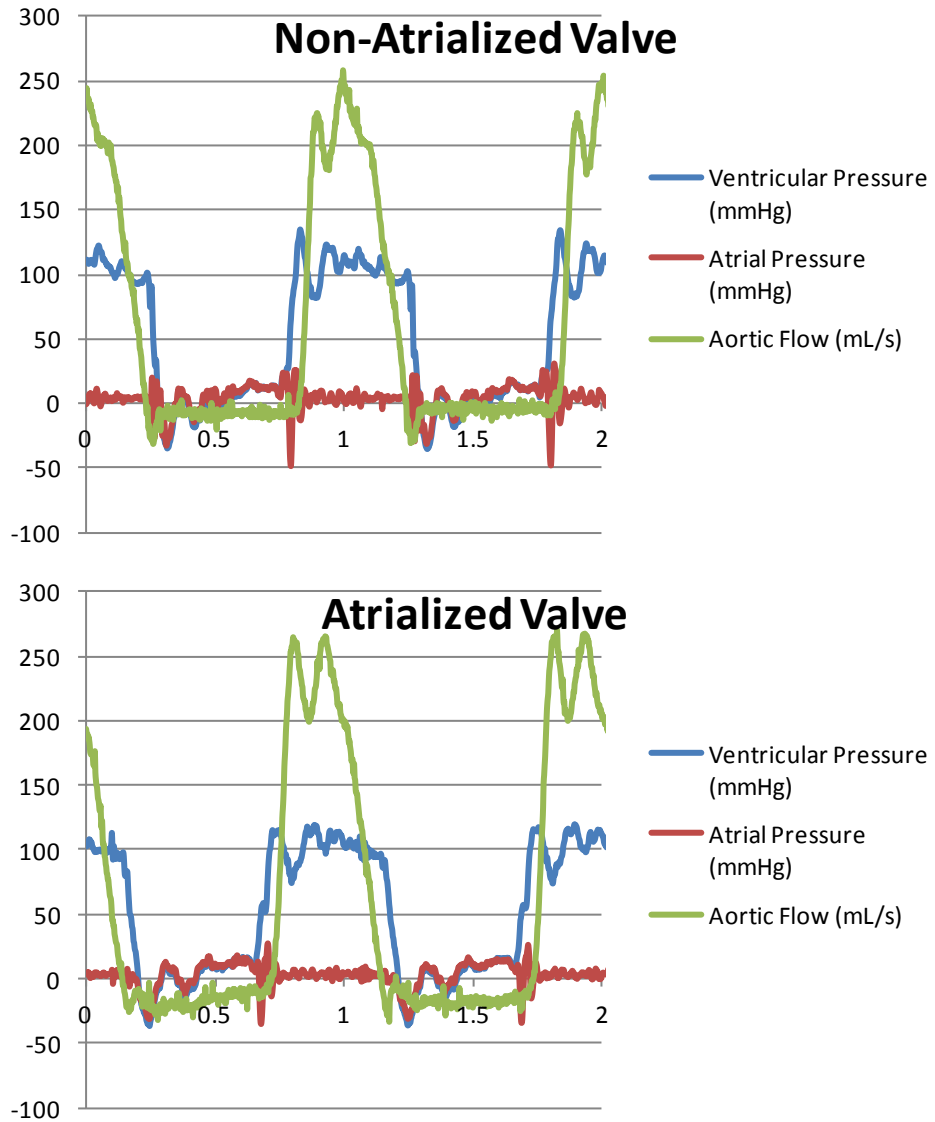


**Figure 21. Pressure and flow wave forms for each valve design at a heart rate of 60 beats per minute and cardiac output of 5 liters per minute**

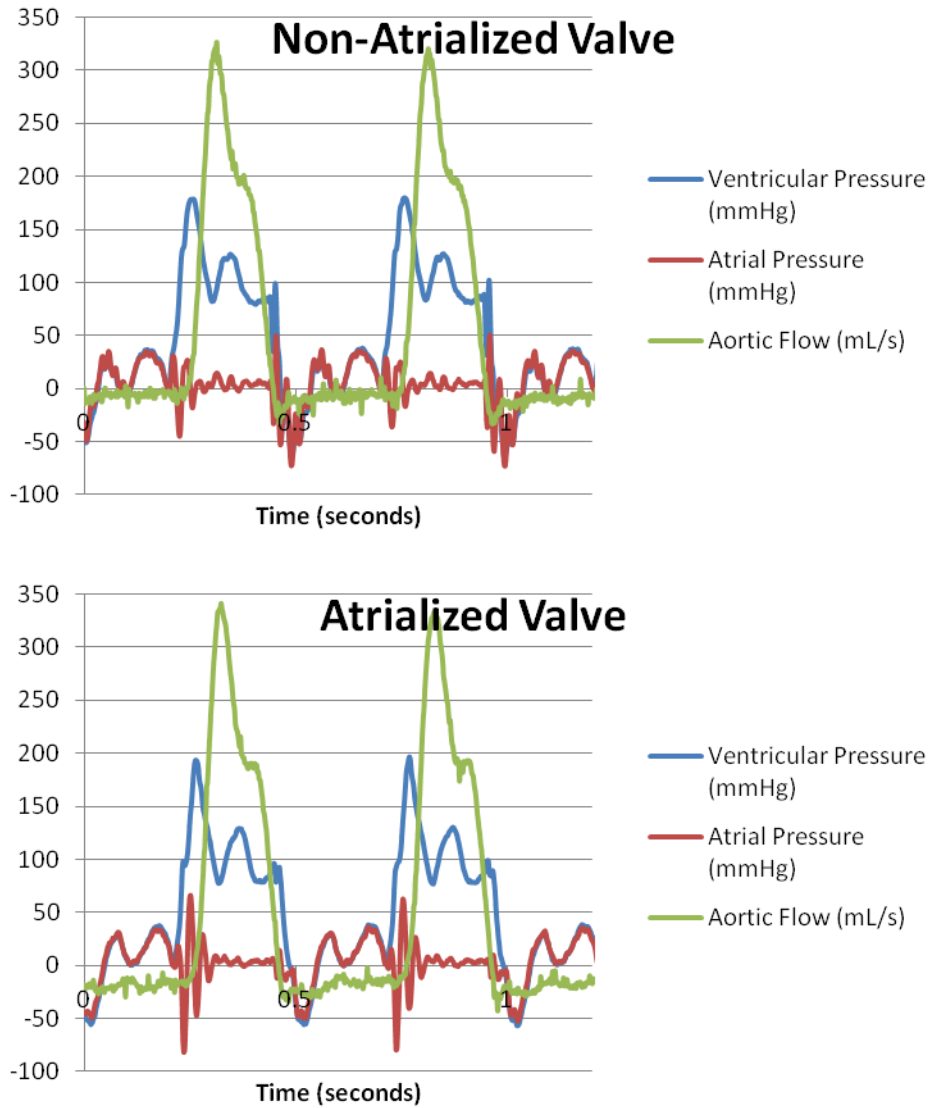


**Figure 22. Pressure and flow wave forms for each valve design at a heart rate of 120 beats per minute and cardiac output of 5 liters per minute**

### 3.3.2 GOA and leaflet kinematics

The results of the GOA calculations were  $2.46 \pm 0.04 \text{ cm}^2$  for the atrialized leaflet design and  $2.68 \pm 0.07 \text{ cm}^2$  for the non-atrialized design. The difference between GOA values for the valve designs is statistically significant with a p-value of less than 0.001. The

raw data for these calculations can be seen in Appendix I. The outer diameter of the valve stents were the same when measured, the difference in GOA values appeared to be due to the atrialized nature of one valve design. The portion of the valve leaflets that is atrialized protrudes into the orifice during diastole and during leaflet closure, this portion is free to bulge unrestrained. This bulge during the high pressure closing of the mitral valve is an area that could produce a large amount of stress in the leaflets and had an adverse impact on the long term durability of the valve.

The resulting coaptation of each valve design can be seen in Figure 23. These images are indicative of all cardiac cycles for each valve and reveal proper coaptation for both the atrialized and non-atrialized valve designs.

Opening times for both valves at the start of diastole were approximately 0.08 seconds with closing times being slightly longer at closer to 0.10 seconds.

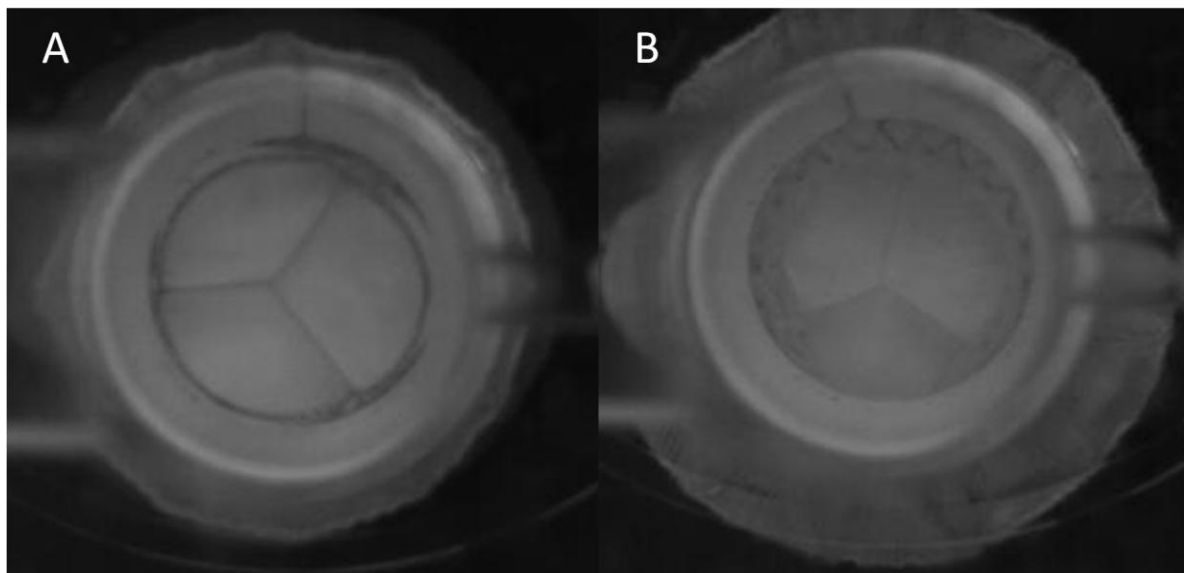


**Figure 23. High speed imaging reveals proper coaptation for both the atrialized design (A) and the non-atrialized design (B)**

### 3.3.3 Flow and Turbulence

Vector fields with contours representing vorticity (red and blue being opposite directions of out of plane vorticity) for each valve at 60bpm (Figure 25) and 120bpm (Figure 26) can be seen in the following figures. In each of the figures below, the fluid flow is moving from left to right and the scale for the vorticity contours is identical between all images.

Fluid flow through the valves begins with leaflet opening and the start of flow through the valve. This results in the formation of an out of plane vortex ring. Eventually the flow becomes unstable with some vortex shedding being seen before the flow begins to decelerate and systole begins.

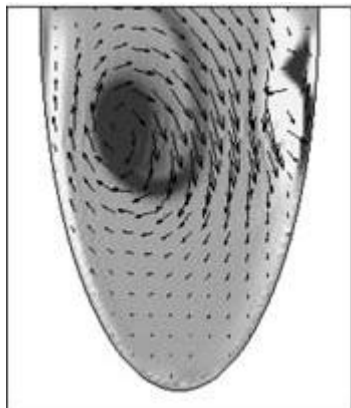


**Figure 24. Computational vector fields resulting from the fluid flow through a healthy mitral valve during diastole [37].**

As can be seen in the figures, the vector fields and vorticity dynamics between the two valve designs are essentially indistinguishable. Analysis of these vector fields shows proper vortex ring formation which is an important feature in the healthy heart. During diastole, a vortex ring forms in the left ventricle. A CFD model of blood flow through a human heart depicts this vortex formation in Figure 24 and is very similar to the vector fields obtained from PIV.

The same vortex fields with contours representing Reynolds shear stresses (RSS), as opposed to vorticity, can be seen in Figure 27 (60 bpm) and Figure 28 (120 bpm). In these figures, the values of RSS are presented in

$N/m^2$ . Accompanying these figures, a table of the maximum RSS and velocity values can be seen Table 1.

Turbulent stresses ranging from 10-100 Pa have been shown to trigger platelet activation; however, activation is also dependent on the time in which the platelets are exposed to this stress. To note, the stress needed to cause hemolysis is much higher than this value and is estimated at greater than 600 Pa [8]. The maximum RSS and velocity values seen in Table 1 are well within the safe ranges for RBC damage; however the valves do have the potential to cause platelet activation.

These data cannot be compared directly to literature results due to the working fluid and non anatomical geometry of the left ventricular block used for testing. It would have been useful to have a control mitral bioprosthesis to compare the TAMI valves to. The small orifice relative to other mitral prosthesis may be a contributing factor to the high RSS and velocity values seen in PIV data.

**Table 1. The resulting maximum Reynolds Shear Stress (RSS) for each valve under a range of heart rates. Each valve and heart rate was tested at a cardiac output of 5 liters per minute. Also shown is the maximum velocity for each take from the ensemble averaged velocity field.**

Valve	Heart Rate (bpm)	Max RSS ( $N/m^2$ )	Max $V_x$ (m/s)
Atrialized	60	58.3	1.35
Atrialized	90	70.9	1.57
Atrialized	120	101.9	1.65
Non-Atrialized	60	45.4	1.41
Non-Atrialized	90	69.2	1.32
Non-Atrialized	120	72.5	1.62

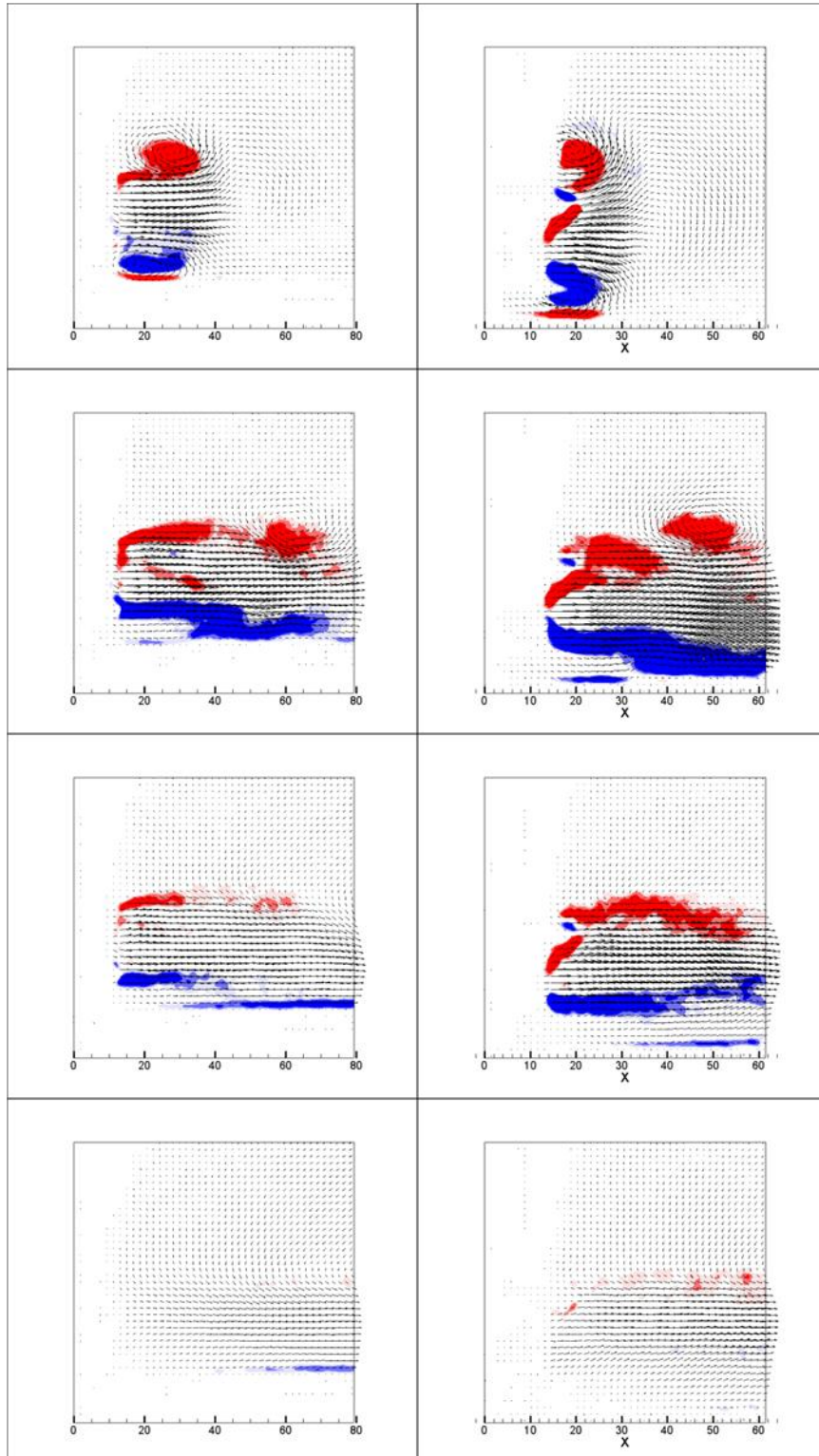


**Figure 25. Vorticity dynamics for each valve at a heart rate of 60 bpm and cardiac output of 5 lpm. The vectors represent velocity and the contours represent opposite directions of out of plane vorticity. The atrialized valve design is on the left and the non-atrialized design is on the right.**

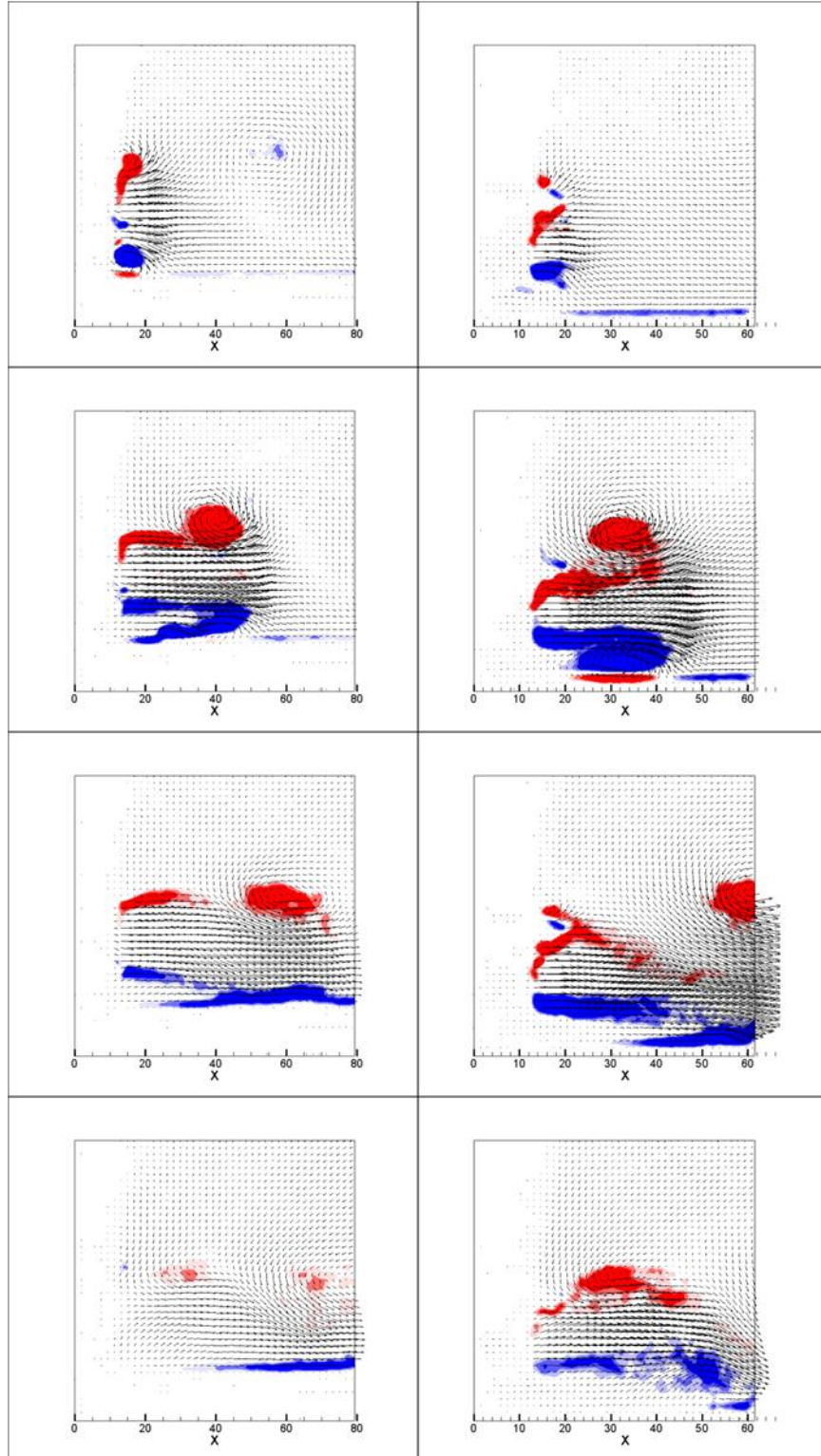


**Figure 26. Vorticity dynamics for each valve at a heart rate of 120 bpm and cardiac output of 5 lpm. The vectors represent velocity and the contours represent opposite directions of out of plane vorticity. The atrialized valve design is on the left and the non-atrialized design is on the right**

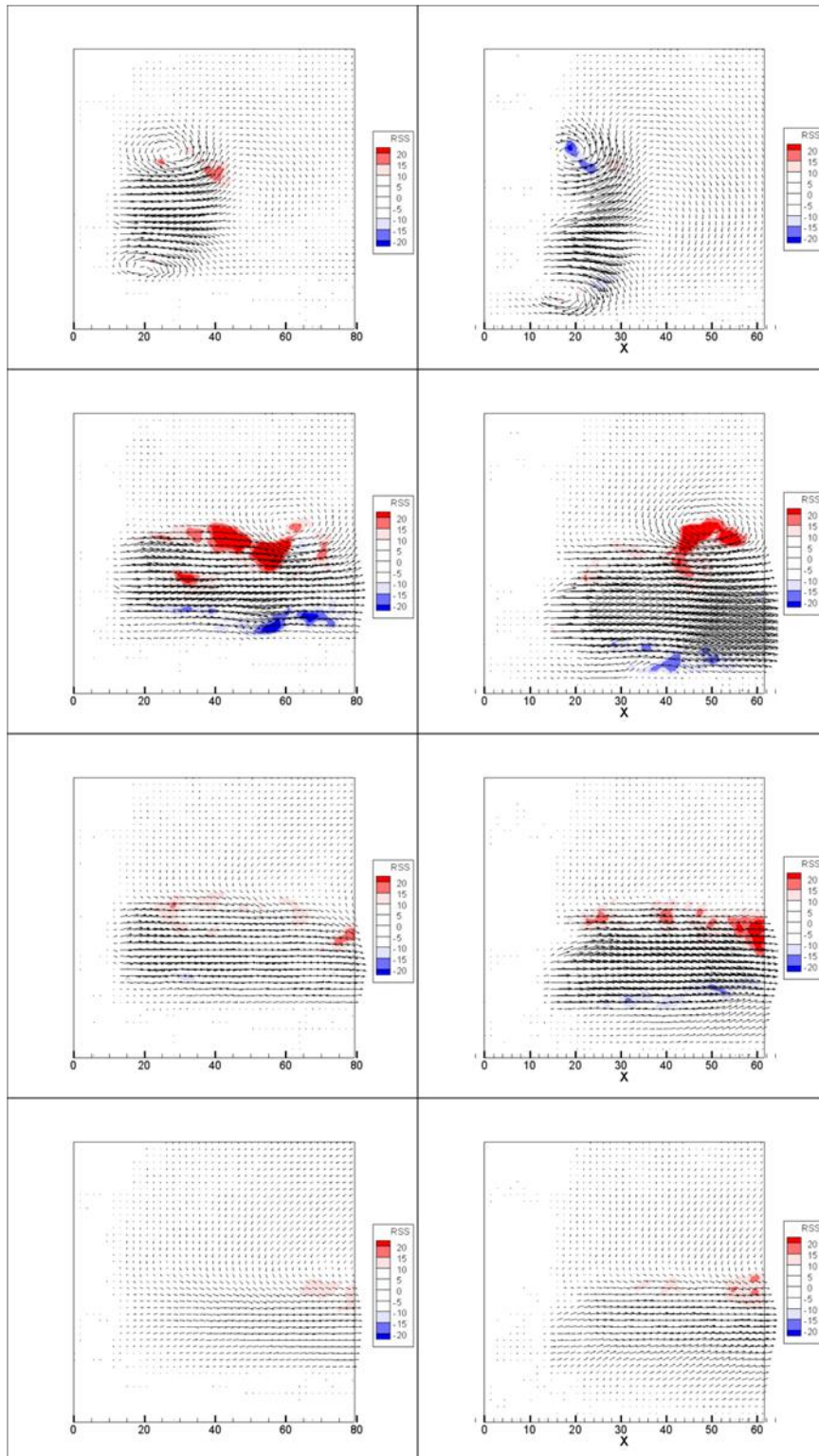


**Figure 27. Vector fields with contours representing Reynolds shear stress ( $\text{N/m}^2$ ) throughout diastole for a heart rate of 60bpm and cardiac output of 5lpm. Atrialized valve design is on the left and the non-atrialized design is on the right. Images go in sequence from the beginning of diastole (top) to the end of diastole (bottom).**

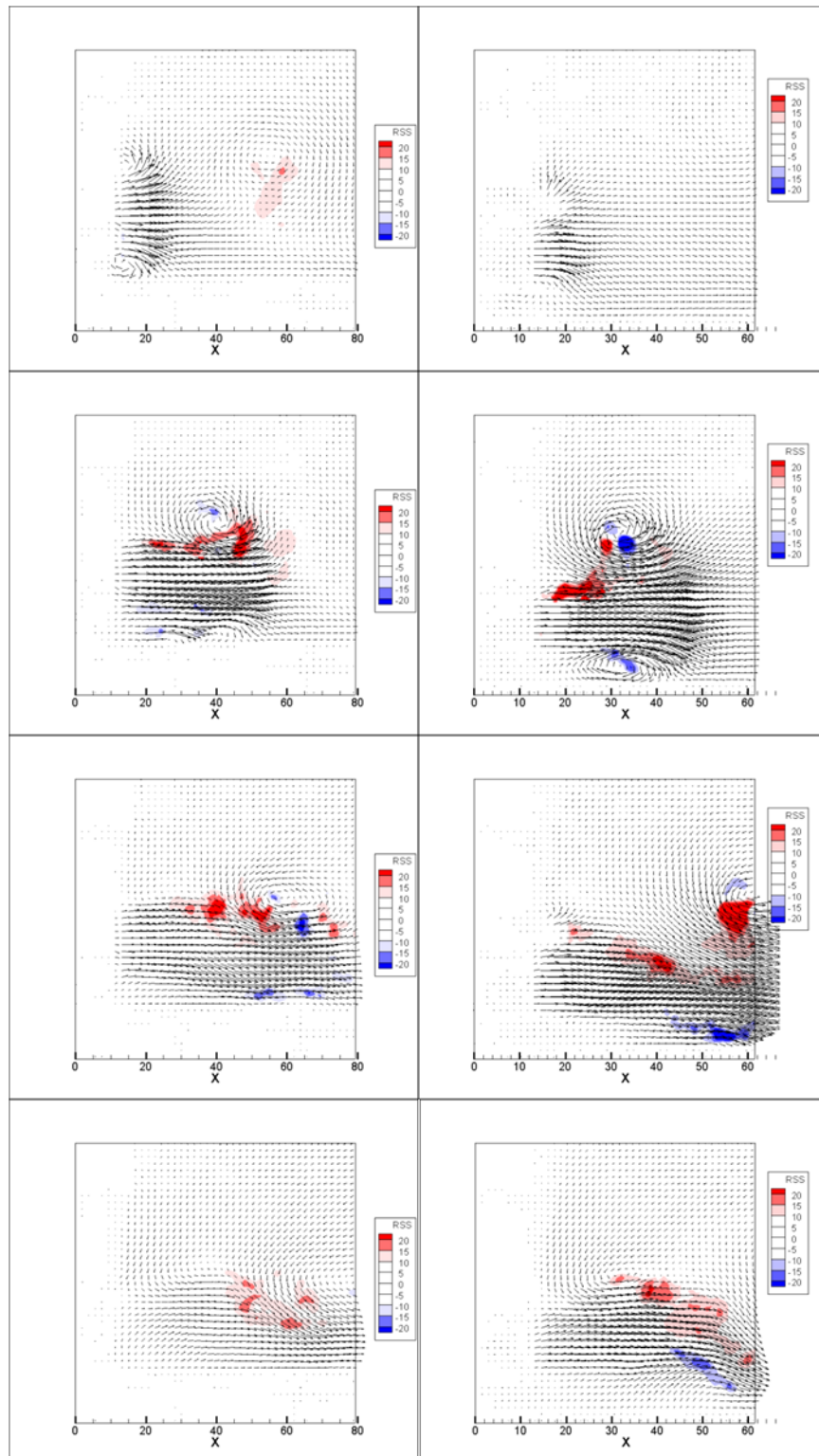


**Figure 28. Vector fields with contours representing Reynolds shear stress ( $\text{N/m}^2$ ) throughout diastole for a heart rate of 120bpm and cardiac output of 5lpm. Atrialized valve design is on the left and the non-atrialized design is on the right. Images go in sequence from the beginning of diastole (top) to the end of diastole (bottom).**

## Chapter 4: Aim 2 - IVBHS and implantation

### 4.1 Chapter Introduction

Aim 2 is to evaluate and understand the differences in mechanics between two different methods of ventricular fixation in transapical mitral valve implantation. In this experimentation, two differing methods of ventricular attachment will be assessed: Tethering and hooking. As described previously, the valves used in this study were designed to be implanted with tethering as the primary means of ventricular fixation, so the designed method of implantation will be used during tethered implantation of the valve into the porcine test sample.

In tethered trans-apical valve implantation, the valve's atrial cuff and stent body are sequentially released into the left atrium and mitral annulus respectively. The tethers are then individually tensioned and secured to the myocardial tissue of the left ventricle in close proximity to the apex of the heart. The tensioning of this process is done using medical imaging to minimize PVL, MR, and LVOT obstruction. Once this has been optimized, the tethers are secured permanently.

For the second method of fixation, it is not an option to alter or produce new valve stents with hooks, so a differing method will be used to closely replicate the hooking method. The valves will be sutured into place, using the same anatomical locations for placement as seen in the Tiara mitral valve developed by Neovasc, Inc.

The primary measure of concern is paravalvular regurgitation. There are two means of regurgitation through prosthetic heart valves: central regurgitation and paravalvular

regurgitation. Central regurgitation occurs when the leaflets do not have proper coaptation and allow blood to pass in a retrograde fashion through the valve.

Paravalvular regurgitation is when blood passes through an orifice other than that in which the leaflets reside. This type of leakage is sometimes seen in standard open heart implanted prostheses, but is seen more often and is considered more of a problem with minimally invasive valves. Minimally invasive valves typically rely on radial force or other means as fixation methods, whereas conventional valve replacements often have a suture ring directly attached to the valve. This opens the minimally invasive options to paravalvular regurgitation: Anytime there is a non-uniform expansion of the stent or incomplete seal of the cuff against the native tissue, there exists a possible orifice for PVL to occur

Due to the anatomical constraints of the mitral valve – as discussed in a previous section – the valves cannot use radial force as the primary means of fixation. Two alternatives to this are being investigated in the following pages.

## 4.2 Aim 2 Methods

### 4.2.1 In Vitro Beating Heart Simulator

For this portion of experiments a passively beating heart simulator, known as the in-vitro beating heart simulator (IVBHS) was used. The system is made up of five main components; a diaphragm pump, porcine test section with accompanying adapters, data acquisition and control, flow control and fluid reservoir. The schematic for the IVBHS can be seen in Figure 29.

The diaphragm pump is a pneumatic design consisting of a large rigid acrylic cylinder with an acrylic flange on one end that allows attachment to a thin walled flexible tube. This flexible tube is capped on the either end to prevent any fluid leakage. The large acrylic cylinder is compressed against the cylinder end and the other end of the cylinder is capped as well, resulting in a sealed pressure vessel. The pressure vessel has two 13mm holes with acrylic tubes that are connected to Tygon tubes that go to one of two different solenoid valves. One solenoid valve is connected to a vacuum line while the other is connected to a high pressure air line. The pressure in the air line is controlled using a pressure regulator that is upstream of the solenoid valve.

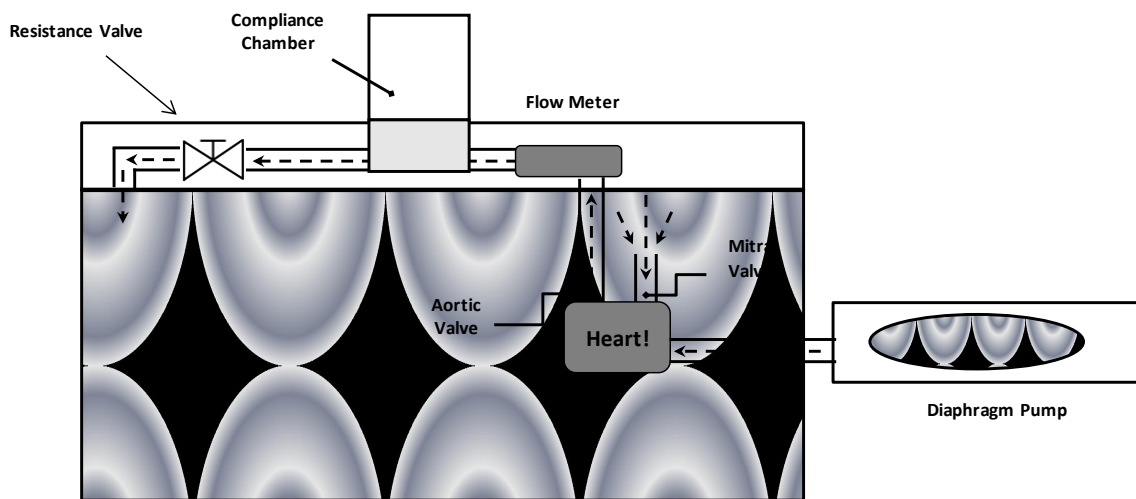


**Figure 29. Schematic of the In Vito Beating Heart Simulator (IVBHS).**

Air pressure is used to create the pumping action within this diaphragm pump. When the vacuum line is active, the flexible membrane expands, drawing water through the mitral valve and into the diaphragm pump. The high pressure air line is then activated – while simultaneously the vacuum line is deactivated – which results in a compression of

the flexible tube and expels fluid out of the pump and back into the left ventricle of the porcine test section.

The porcine test section is immersed in a tank and held in place by specifically designed aortic and ventricular adapters (the porcine test section and preparation is described in depth in its own section). The test section is immersed for several reasons. An early design iteration of this system needed passive actuation of the mitral valve, which the column of water above the immersed section provided. A second reason is that immersion allows the entire left atrium to be removed and the mitral valve, fully visualized. This allows for complete access to and view of the mitral valve; which is necessary for proper visualizing and placement of any mitral valve prosthesis (or repair device) without the need for complex medical imaging.

Upstream of the aortic adapter and downstream of the ventricular adapter there are fittings that allow for the insertion of 3mm OD thin walled nylon tubing. The end of the tubing has been thermally welded and 1.5 mm diameter ports are upstream at 5 mm increments and 90 degrees from each other. These tubes lead to pressure sensors that allow for the real time measurement of ventricular and aortic pressure. The tubing length has been measured specifically such that the pressure taps are located 3-5mm inside of the left ventricle and 5-10 mm downstream of the aortic valve. The ventricular adapter is attached to the tube leading to the diagraph pump and the aortic adapter is attached to the tube leading to the flow meter, compliance chamber and resistance valve.

An in-line flow probe downstream of the aortic valve as well as a clamp-on flow probe upstream of the ventricular adapter allows for measuring of flow rate through the system without any significant pressure drops. The inline flow probe is held in place using hose clamps between two pieces of tygon tubing. The clamp-on flow probe has been design and calibrated to clamp onto the outside of 1 ¼ inch tygon tubing.

The in-line flow meter is connected downstream from the compliance chamber which is used to simulate the compliance of the systemic cardiovascular system due to the flexibility of both arterial and venous walls. The compliance chamber is an acrylic cylindrical chamber that receives fluid from the flow meter at its inlet and its outlet leads to the flow control valve. The cylinder is sealed, except for two taps at its top; one leads to a pressure gauge and the other to a bulb pump. Compliance is varied by varying the amount of air in it using the bulb pump: more air in the chamber results in more compliance and less air results in less compliance. The amount of compliance is modulated to ensure proper pressure ranges in the system to emulate physiologic conditions. A simple ball valve has been placed downstream of the compliance chamber in order to finely modulate the amount of flow. The ball valve can be finely tuned to build up proper pressures within the system and gain proper flow conditions.

Table 2 contains detailed information about each of the flow probes and pressure transducers used during experimentation using the IVBHS.

**Table 2. Detailed information regarding flow probes and pressures sensors used during IVBHS experimentation.**

Item	Company	Model
In-Line Flow Probe	Transonic Systems, Inc (Ithica, NY)	ME 25PXN
Clamp-On Flow Probe	Transonic Systems, Inc (Ithica, NY)	ME 20PXL
Flow Meter	Transonic Systems, Inc (Ithica, NY)	Model T402
2 x Pressure Sensor	Validyne Engineering Corp. (Northridge, CA)	DP15-34

#### 4.2.2 DAQ and Control

The IVBHS is both monitored and controlled using a custom LabVIEW VI designed and created for this purpose. The VI records data from both pressure transducers and one ultrasonic flow meter at a time (either the in-line or clamp on – but not simultaneously) and sends user controlled signals to the two solenoid valves that control the diaphragm pump.

The VI displays – both graphically and numerically – systolic and diastolic pressures; mean arterial pressure; and cardiac output. The VI allows the user to control the heart rate and duty cycle; the other parameters must be adjusted using the compliance chamber and resistance valve physically located on the IVBHS.

The LabVIEW VI also allows the user to collect all pressure and flow data for a specified period. This allows for precise measurements of pressure and flow curves for each

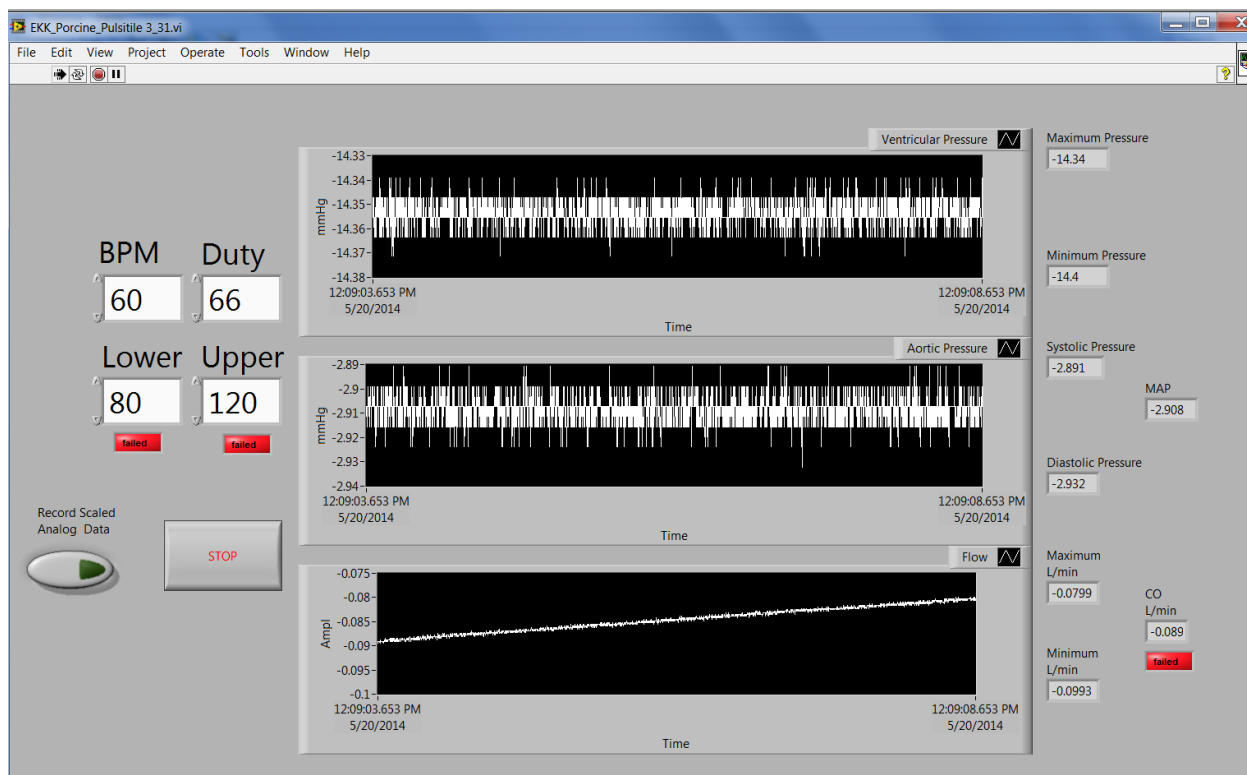


**Figure 30. LabVIEW VI built to control the In Vitro Beating Heart Simulator (IVBHS). User input fields include heart rate and duty cycle as seen above. The VI also includes a data acquisition toggle button as well as graphical displays of the following: Ventricular Pressure, Aortic Pressure, and Flow Rate.**

transducer. A screen shot of LabVIEW VI showing all control and output fields can be seen in Figure 30.

#### 4.2.3 Heart Preparation

Porcine hearts were harvested according to our specifications and were received from the abattoir as seen in Figure 31. Any cuts or damage to the exterior tissue of the heart as a result of the harvesting process or transportation resulted in the heart being disposed of. The hearts were stored in phosphate buffered saline at a temperature of 2 – 4 °C from immediately after being gathering until used in experimentation.

Before experimentation, each heart was prepared in the same manner. All extraneous tissue was removed. The removed tissue included: Any pericardium, non-cardiac tissue remaining attached to the heart, left and right atrium, pulmonary artery, and any fatty deposits on the aorta. When removing the left atrium, enough tissue was left for the atrial cuff of the implanted bioprostheses to seat properly. In some instances, the remaining atrial tissue would begin to occlude the opening to the mitral valve. In these cases, the remaining atrial tissue was lightly pulled back and secured to outside of the heart using sutures. Care was made to not affect the annulus geometry by tensioning the atrial tissue to a high degree. The aorta was then trimmed, leaving approximately 25mm of aortic tissue downstream of the aortic valve commissures and the coronary



**Figure 31. Porcine heart as received from the abattoir, before extraneous tissue has been removed.**

arteries were tied off with sutures to prevent any coronary flow. Ports were inserted into the left ventricle and the remaining aorta in order to attach the heart into the IVBHS.

The aortic adapter consisted of a thin walled-acrylic tube. On one end, the adapter is the same diameter as the Tygon tubing to which it was attached and the other end was approximately the same ID as the aorta.

Several aortic adapters were made to correspond to varying aortic sizes in the

porcine test sections. Two nylon tie wraps are positioned next to each other along the axis of the adapter around the portion of the aorta with the adapter inserted in it. The tie

wraps are then tightened. The larger diameter portion of the adapter is then inserted in the Tygon tubing and fixed into position with hose clamps.

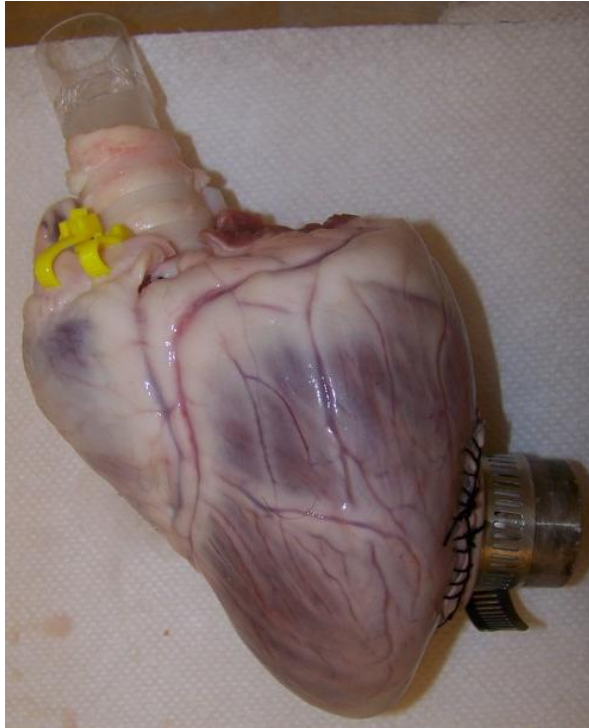


**Figure 32. Fully prepared porcine heart for use in the IVBHS. Ventricular port is seen on the right while the aortic port is seen on the top of the heart.**

The ventricular adapter was of custom design. It has 3 main parts; a tapered section, a cylindrical section and a flange. The inside diameter of the adapter is 25.4 mm and the length is 50.8 mm. The two sections are sub-divided by the flange which is 38.1 mm in diameter and 1 mm thick. A circular piece of polyester fabric approximately 76 mm with a 25 mm hole in the middle is fitted over the cylindrical portion of the adapter and held in place with a tie wrap. The tapered end is inserted through a hole in the left ventricle

the size of which is equal to the smallest outside diameter of the tapered section, approximately 26 mm. When creating this hole in the left ventricle, the ventricular adapter itself is used as a 'corer.' A surgical blade and forceps are used to cut through any remaining intact myocardial tissue. Great care is used at this point to ensure that the native mitral apparatus is left as undamaged as possible. It is important to be sure that the native papillary muscles and chordae tendinae remain largely intact to ensure proper left ventricular geometry. The adapter is then held in place against the exterior wall of the left ventricle using a continuous suture technique through a polyester fabric

ring and the exterior wall of the left ventricle. The fabric and suture force the flange and taper against the tissue and seal the adapter to the heart so that minimal fluid leaks from the heart as the left ventricle is pressurized. The cylindrical portion of the adapter is inserted into Tygon tubing coming from the diaphragm pump and held in place with a hose clamp. Figure 32 shows a properly prepared porcine heart as used in experimentation.

#### 4.2.4 Valve Implantation

Firstly, each of the 3 tethers is threaded through one of the three eyelets on the stent body. The tether attachment can be seen in Figure 33. Then a small hole approximately 2.5 mm in diameter was created at the apex of the heart. This hole extends through the entirety of the myocardium and into the left ventricular cavity of the porcine heart. Forceps were used to securely grasp all of the tethers and then advance them through the previously created hole at the apex of the heart. The forceps were advanced carefully so as not to cause any further damage to the myocardial tissue. Once through the hole, the tethers were grasped using another set of forceps while the original set released hold of the tethers and were retreated back through the hole in the apex. The stent body was then inserted into the mitral annulus by hand while the tethers were simultaneously tensioned to ensure proper securing of the prosthesis within the mitral annulus. The tethers were then temporarily secured outside the apex of the heart using forceps.

After proper implantation of the bioprosthesis, tether tension is optimized in the IVBHS. Real time measurement of cardiac output, tactile feel, and visualization of the prosthesis were used to optimize the tension. Once a moderate cardiac output was attained in the

IVBHS, tether tension was modulated until PVL detected by tactile feedback using a gloved hand was minimized and cardiac output was maximized. The prosthesis was also visualized during this procedure to ensure that the valve had not been pulled through the annulus and into the left ventricle. The tethers were then secured using locking forceps at the apex of the heart.

Sutured implantation begins with the preliminary placement of the attaching sutures;



**Figure 33. The orientation and attachment points of the tethers on the larger profile stent valve. The attachment points are look identical on the valve design that contains more atrialized leaflets.**

Ethicon silk 2-0 sutures were used for all implantations. Three suture points were selected to secure each valve: Two positions on the anterior leaflet and one on the posterior. The attachment point on the posterior leaflet was centrally located on P2, while those on the anterior leaflet were laterally located at A1 and A3. At each of

these attachment points, a suture was looped around at least one primary chordae (those that attach to the free edge of the leaflet). The suture needle was removed and one end of the suture was fed through each attachment points' respective eyelet in the stent body. Both free ends of the suture were pulled through the center of the valve to enable implant of the valve in the mitral annulus. The valve stent body was properly oriented, compressed and then placed within the mitral annulus and released.

Assuming proper orientation and placement of the prosthesis, the suture associated with each attachment point was knotted multiple times to ensure a tight and secure fit.

Each heart was implanted with both valve designs in the sutured fashion so great care had to be taken when removing an implanted valve to ensure that the chordate tendinae used for fixation remained unharmed. Small surgical scissors were used to cut the knot at each attachment point and remove the valve.

Figure 34 shows each valve design implanted as seen from the atrium. These particular valves were implanted in the sutured fashion; however, both methods of implantation appear identical when viewed from the atrium. The atrialized design can be seen on the right while the non-atrialized design can be seen on the left.

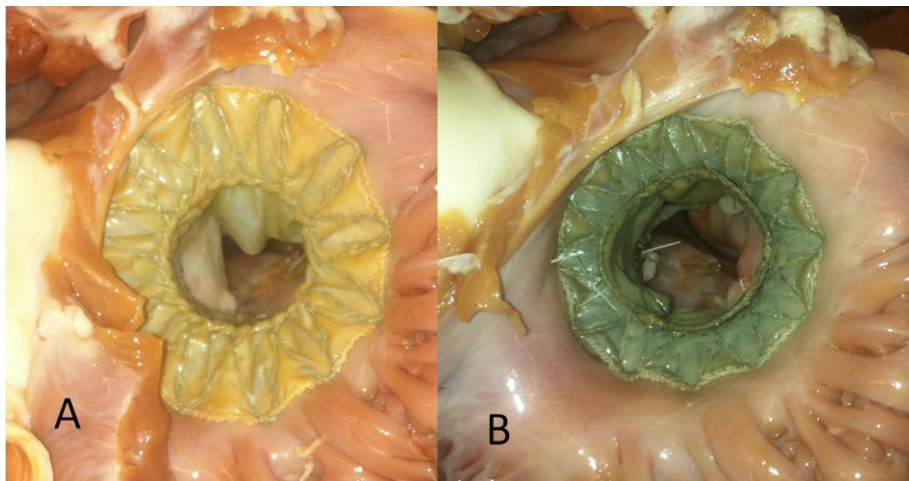


**Figure 34. Each valve design implanted as viewed from the left atrium. A) Larger stent profile design with the larger atrial cuff. B) Atrialized stent design with smaller cuff.**

#### 4.2.5 Data Measurements and Calculations

The annulus was measured both manually and using Doppler ultrasound. The manual measurement was performed using custom made measuring devices. The measuring

devices were created in increments of 1mm ranging from 18mm to 32mm. This was sufficient in measuring all of the hearts that were collected. Annular measurements using the ultrasound were performed on captured images at the peak opening of the mitral valve. Two different annulus diameters were recorded: septo-lateral and intercommissural. Mitral annulus measurement is typically performed using a sizing toolset provided specifically by each manufacturer that correspond to sizes of their specific device; however, the septo-lateral and intercommissural measurements are two important measurements when determining the proper mitral valve size. An example of a mitral valve sizing tool and the measurements that are made with the tool are shown in Figure 35. The valve sizing tool typically corresponds to a specific size of valve or annuloplasty ring manufactured by the company; however, they also measure the intercommissural distance, total area of the mitral valve and the septo-lateral distance [38].

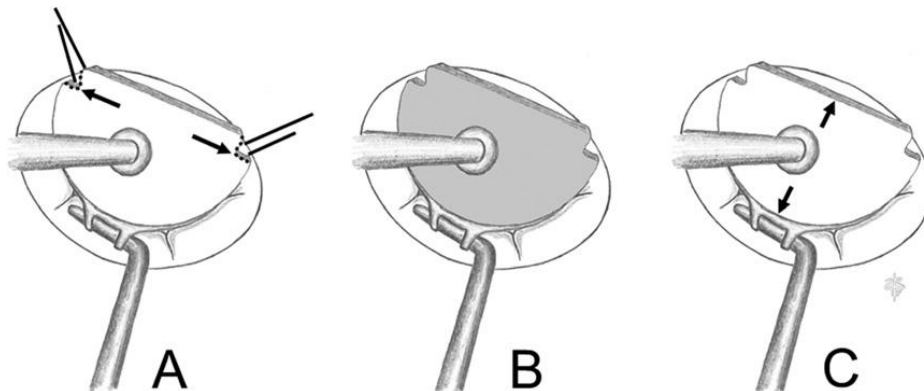


**Figure 35. An example of a mitral sizing tool used by surgeons. The tool can be used to measure the intercommissural distance (A), the total area of the valve (B) and the septo-lateral distance (C) [38].**

For each porcine heart, flow and pressure data was collected for five different conditions. These conditions comprise each of the two valves in two different

implant methods – tethered and sutured. In addition to these four conditions, data was acquired for the heart with normal function of the native valve. For each of the five conditions, 20 cardiac cycles of data were collected. Ten sequential cycles utilizing the in line flow probe – or aortic flow – and ten sequential cycles utilizing the clamp on flow probe – or total flow. In addition to flow measurements, aortic and ventricular pressures waveforms were captured for each cardiac cycle. All of these measurements are made at 500 Hz.

The measurement of primary concern is the flow. For each flow meter and each cardiac cycle, numerical integration was performed in Microsoft Excel to calculate the forward volume expelled during each cardiac cycle. Integration of the aortic flow profile results in a typical stroke volume seen in cardiac mechanics: This can be seen as the blue area minus the red area in Figure 36A. Integration of the clamp on flow profile, however, results in a total stroke: This can be seen as the blue area in Figure 36B. The difference of these two strokes is interpreted as the volume of fluid that is lost in the system, i.e. the amount of fluid that is expelled by the diaphragm pump, but does not pass through the aortic valve.

This volume of fluid has the potential to be lost in several places: closing mitral valve leakage, central mitral regurgitation, leakage through the ventricular port attachment, trace flow through the coronary arteries and PVL. As seen in Aim 1, the bioprosthesis appear to have proper leaflet coaptation that results in no central leakage. The ventricular port leakage, coronary artery flow, and closing valve leakage are assumed to be unchanged between conditions for a given porcine test section. Thus, only PVL is responsible for changes in fluid volume loss between valve treatments for each heart.

In order to compare the resulting PVL changes between valve treatment groups, a mitral regurgitant fraction (MRF) value was calculated for each condition. The MRF is equal to the mitral regurgitant volume divided by the total stroke. The regurgitant volume is calculated by subtracting the forward aortic volume during systole from the

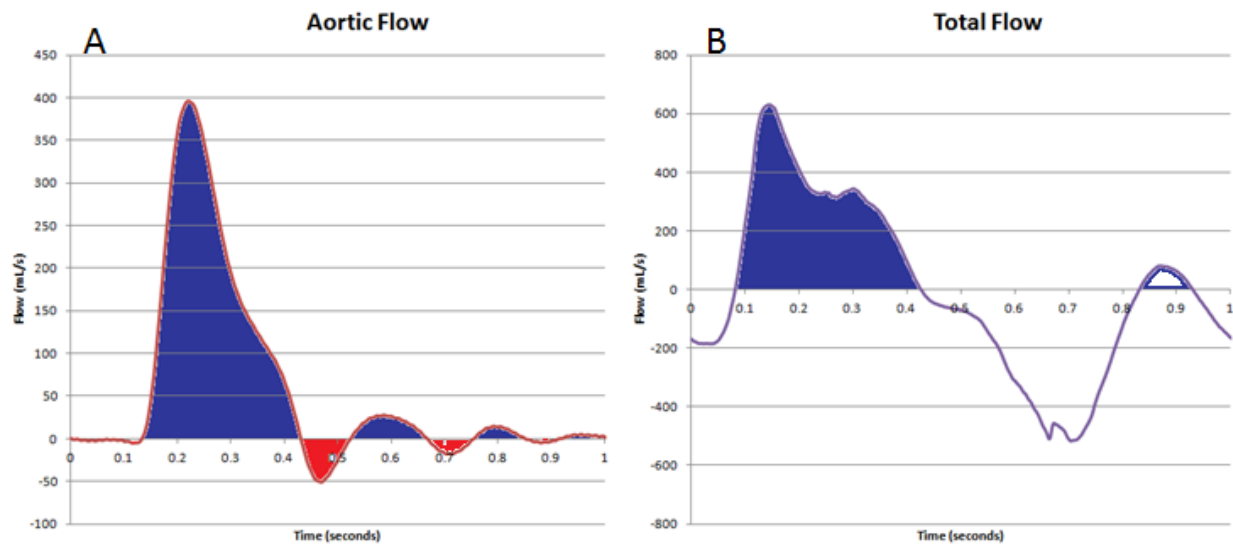


**Figure 36. Flow profiles and illustration of area under the curve for aortic flow probe (A) and total flow probe (B). In (A) the blue area minus the red area results in the standard stroke volume while the blue area in (B) corresponds to the total forward stroke.**

total forward stroke. The aortic flow during systole can be taken as the area under the first large peak seen in the flow waveform. A larger MRF value indicates a worse performing valve than a lower MRF value: An MRF of 1 indicates that the entire total forward stroke was regurgitant volume while an MRF of close to 0 would indicate a valve with very little regurgitant volume. All volumes calculated from flow curves are based on the averaging of 10 cardiac cycles.

During all experiments, water was used as the working fluid in the IVBHS. In vivo, the working fluid flowing through the heart would be blood which has a much higher viscosity than water. In order to gain a better understanding of what the mitral MRF would be in an in vivo environment, the MRF was scaled for the change in viscosity.

Assuming laminar flow in relatively small regurgitant orifices, the volume scales linearly as compared to velocity. The relative velocity for blood was assumed to be 3.5 for this scaling, thus the regurgitant volumes were divided by 3.5. A small regurgitant orifice for the native condition could not be assumed because of the varying degree of regurgitation so it was not included in the statistical testing after the viscosity correction was completed.

During IVBHS experimentation, a GE Vivid 7 Dimension ultrasound machine was used to perform Doppler imaging. This imaging was used to measure maximum annulus size as well as to image the native and bioprosthetic valves after implantation.

#### 4.2.6 Statistical Analysis

The Mann-Whitney U statistical test was used to test the statistical significance of values between measurements.

Error bars in graphs and figures represent one standard deviation in either direction from the mean and values are represented as the mean plus or minus one standard deviation.

#### 4.3 Results and Discussion

The raw MRF for each condition can be seen in Table 3 and Figure 37. The data after the viscosity correction can be seen in Figure 38 and Table 4. A box plot of consolidated MRF values from each heart can be seen in Figure 37 and data for all hearts can be viewed in Appendix II.

Statistical testing produced the following results. Lumping both conditions for the atrialized valve and the non-atrialized valve resulted a two-tailed p value of 0.037,

suggesting that the atrialized valve performs better. The p value for non-atrialized vs. atrialized sutured implant was 0.047. These p values suggest that as a whole, the atrialized valve performs better, but especially in sutured implantation.

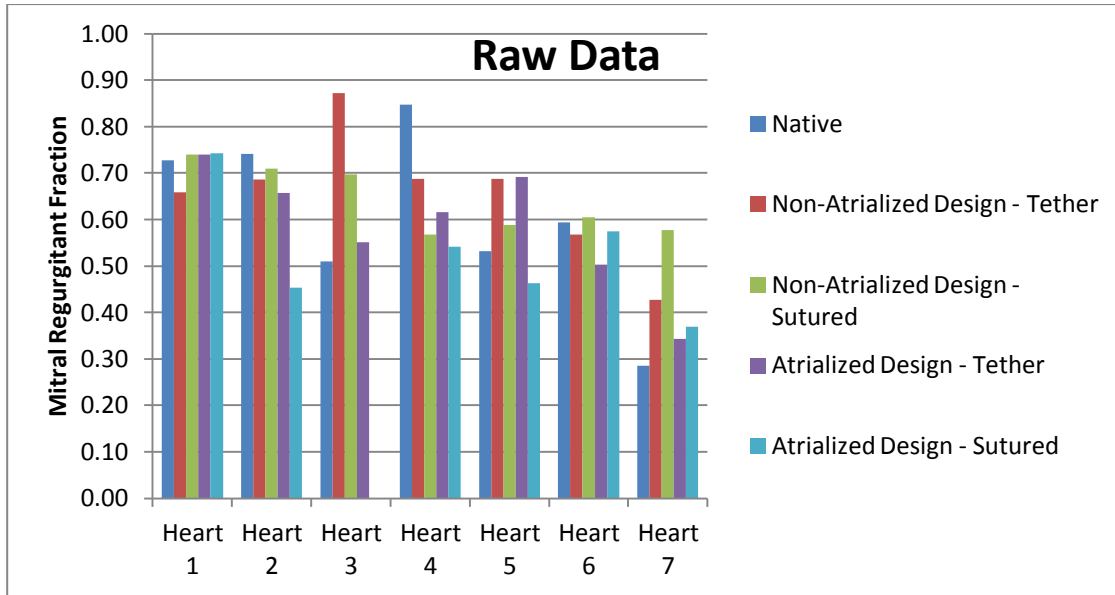


**Figure 37. A column plot of the resulting mitral regurgitant fraction (MRF) for each heart and valve condition.**

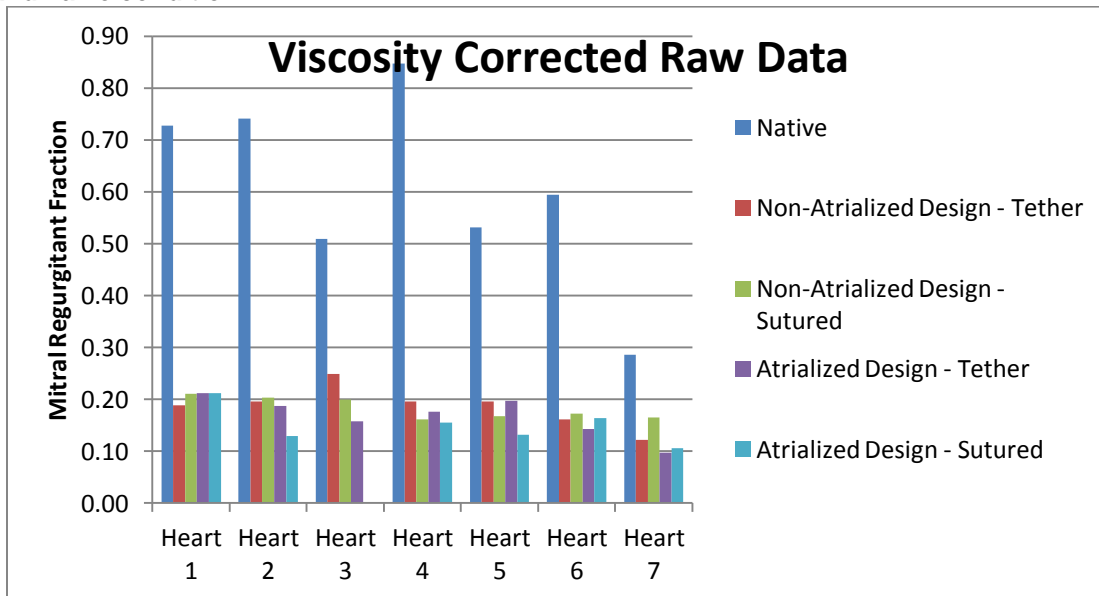


**Figure 38. A column plot of the mitral regurgitant fraction (MRF) for each heart and condition after the viscosity correction has been completed.**

Statistical testing confirmed what was observed during experimentation. With both implant conditions lumped for each valve design, the non-atrialized design proved inferior to the atrialized design. Also, when implanted in the sutured fashion, the non-atrialized valve design resulted in a greater amount of PVR, likely due to a poor sealing of the atrial cuff. When comparing purely the tethered implantation between valve designs; however, the results were not statistically significant.

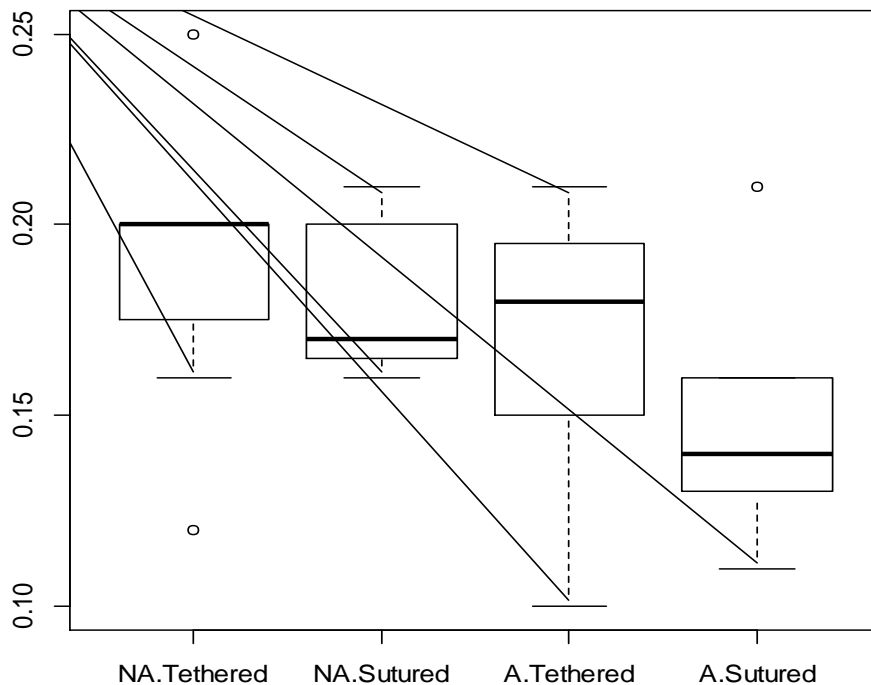


**Figure 39. A box plot representing the viscosity corrected MRF values for each valve condition. NA represents the non-atrialized valve design and A represents the atrialized valve design. The native condition was left out because there is not a suitable viscosity correction for the condition.**

Relatively loose atrial fixation was noted in several cases of sutured implantation of the non-atrialized valve design. It is believed that the distance from the free edge of the

leaflet to the atrial floor is not great enough to result in a secure fit of the atrial cuff: Meaning that the stent height is too great for the heart in which the prosthesis was implanted. Figure 44 illustrates the difference in atrial fixation during systole and diastole of an implanted non-atrialized valve: Figure 44A shows a gap forming between the atrial skirt of the valve and the atrial floor while Figure 44B shows the same gap disappearing during diastole. This same effect was not seen when implanting the non-atrialized valve in the tethered fashion due to the ability to tension the valve manually instead of relying on the position of the native mitral leaflets. It was also not observed in the atrialized valve design. This is likely due to the fact that the distance from the atrial cuff to the fixation point of the stent is significantly less than that of the non-atrialized design. This results in a much more secure fixation in the implanted hearts. A cartoon of this effect can be seen in Figure 40. When secured at the top of the stent body, as was done during implantation, the atrial cuff of the non-atrialized design does not secure well to the atrial floor while the cuff of the atrialized design does.

Although statistical testing only confirmed one observation made during testing, several other parameters were determined to be important in a properly functioning TAMI valve. In either method of attachment, it is apparent that the combination of the stent height profile and ventricular fixation method together play a very important role in the function of the bioprosthesis. Functional problems due to the interaction of these two parameters presents itself in several different fashions, these include: LVOT obstruction, native leaflet interference or poor (or loose) atrial fixation. The poor atrial fixation was supported by statistical testing, but the others will still be discussed below.

**Table 3. Tabular results from In Vitro Beating Heart Simulator (IVBHS) experiments. The two different annulus measurements are displayed as well as the resulting mitral regurgitant fraction for each heart under each valve condition. The annular measurement is the maximum measured for each measurement.**

	Heart 1	Heart 2	Heart 3	Heart 4	Heart 5	Heart 6	Heart 7
<b>Annulus (Intercommisural)</b>	31 mm	24 mm	30 mm	28 mm	29 mm	28 mm	28 mm
<b>Annulus (anterolateral)</b>	28 mm	24 mm	24 mm	27 mm	25 mm	26 mm	24 mm
<b>Native</b>	0.73	0.74	0.51	0.85	0.53	0.59	0.29
<b>Non-Atrialized Design - Tether</b>	0.66	0.69	0.87	0.69	0.69	0.57	0.43
<b>Non-Atrialized Design - Sutured</b>	0.74	0.71	0.70	0.57	0.59	0.60	0.58
<b>Atrialized Design - Tether</b>	0.74	0.66	0.55	0.62	0.69	0.50	0.34
<b>Atrialized Design - Sutured</b>	0.74	0.45		0.54	0.46	0.57	0.37

**Table 4. Results from IVBHS experiments after correcting for the viscosity difference between the working fluid and blood.**

	Heart 1	Heart 2	Heart 3	Heart 4	Heart 5	Heart 6	Heart 7
<b>Annulus (Intercommisural)</b>	31 mm	24 mm	30 mm	28 mm	29 mm	28 mm	28 mm
<b>Annulus (anterolateral)</b>	28 mm	24 mm	24 mm	27 mm	25 mm	26 mm	24 mm
<b>Native</b>	0.73	0.74	0.51	0.85	0.53	0.59	0.29
<b>Non-Atrialized Design - Tether</b>	0.19	0.20	0.25	0.20	0.20	0.16	0.12
<b>Non-Atrialized Design - Sutured</b>	0.21	0.20	0.20	0.16	0.17	0.17	0.16
<b>Atrialized Design - Tether</b>	0.21	0.19	0.16	0.18	0.20	0.14	0.10
<b>Atrialized Design - Sutured</b>	0.21	0.13	0.00	0.15	0.13	0.16	0.11

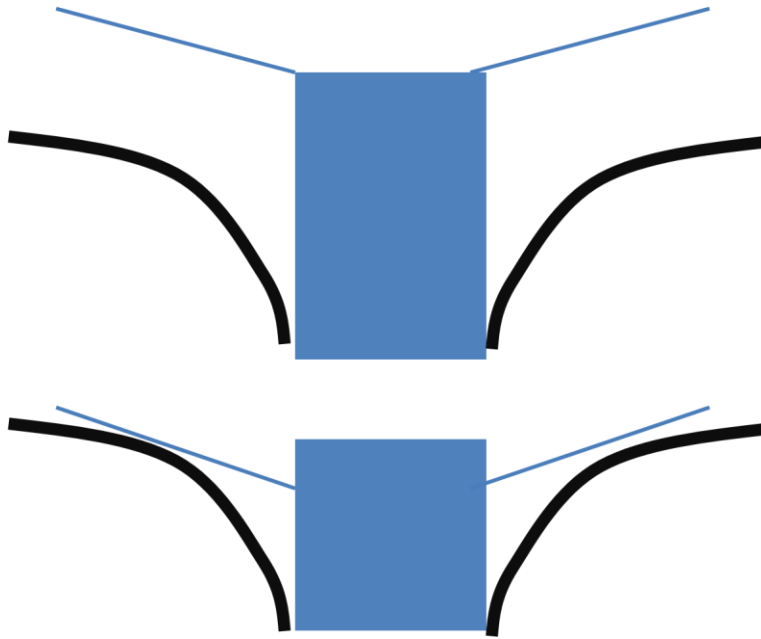


**Figure 40. Cartoon of atrialized vs. non-atrialized suture implantation. Due to the large stent height of the non-atrialized design, the atrial cuff does not secure properly to the atrial floor.**

LVOT obstruction was seen in heart 3 and heart 4 during tethered implantation of the non-atrialized valve. It was also noted in many other hearts whose data did not appear in this report. In the IVBHS, LVOT obstruction presents itself with a much higher diaphragm pump pressure being required to drive the same amount of flow. An image, though hard to distinguish, of LVOT obstruction from the non-atrialized valve design can be seen in Figure 41. Implantation of the same non-atrialized valves in the sutured fashion did not result in any LVOT obstruction. During sutured implantation, the prosthesis position is fixed relative to the native leaflet tissue, thus during systole, the prosthesis is allowed to move with the native tissue to allow more space in the LVOT. No such cases of LVOT obstruction were documented when implanting the atrialized design in either tethered or sutured implantation.

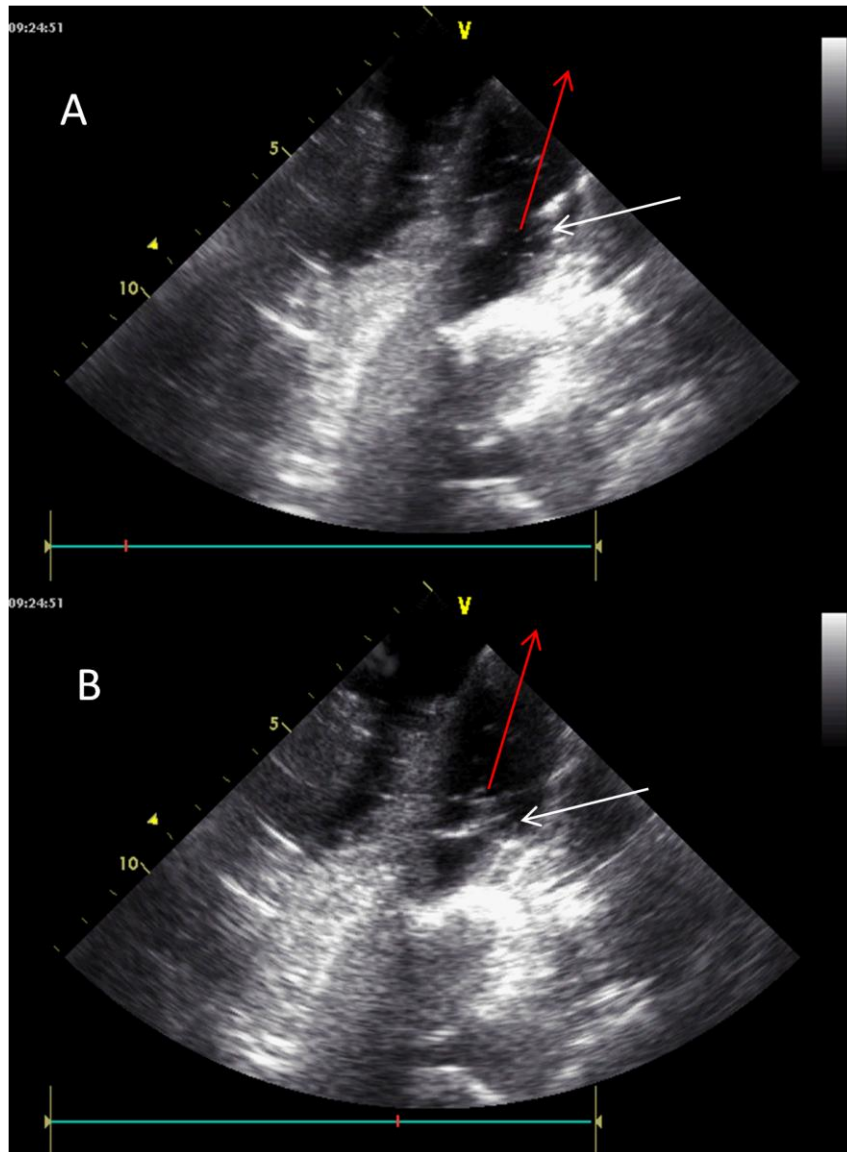


**Figure 41. LVOT obstruction shown during systole (A) and diastole (B). In both images the White arrow indicates the aortic valve and the Red arrow indicates the direction of the aorta. The valve stent can be seen in contact with the inner wall of the left ventricle.**

In many cases, the native mitral leaflets extended beyond the valve stent and began to flap over the orifice of the prosthesis. In some cases, the native leaflets did not experience any degree coaptation and thus had no effect on the bioprosthesis. There were several cases in which the native leaflets maintained near full coaptation and

severely limited the activation of the prosthesis leaflets. An instance of this occurring can be seen in Figure 42: 'A' indicates the closed leaflets of the bioprosthesis and 'B' indicates the closed leaflets of the native mitral valve. A cartoon illustrating this phenomenon more clearly can be seen in Figure 43. This is a Doppler ultrasound image captured from heart 8 described below: In this case, the native leaflets maintained full function. This phenomenon did not result in overall deleterious effects, with the native leaflets maintaining full function, it is believed the prosthesis and the native leaflets worked in tandem to minimize the closing regurgitation experienced by the mitral valve. In these cases, valve implantation typically improved the MRF of the heart, however the values remained virtually unchanged between valve design and

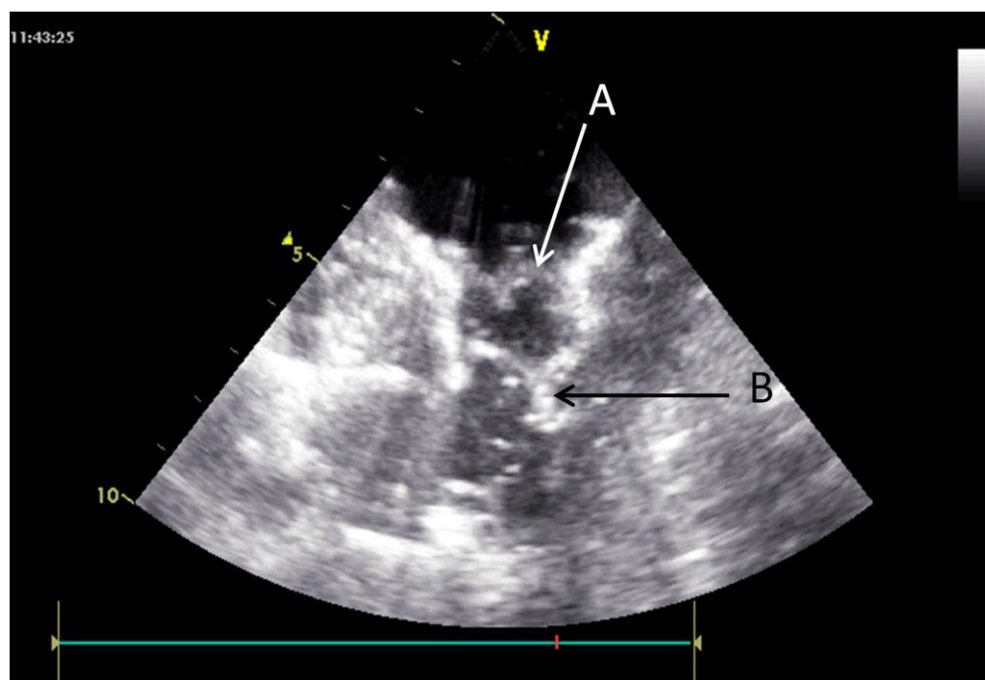


**Figure 42. An occurrence of the native leaflets interfering with bioprosthesis function as captured by Doppler imaging. The closed leaflets of the bioprosthesis are pointed out by 'A' and the closed leaflets of the native mitral valve are indicated by 'B.' In this view, the open area that would be the left atrium can be seen at the top of the image and the valves open into the left ventricle which would be below the image.**

implant method. The occurrence of this phenomenon was seen less with often and to a less severe degree with sutured implantation. During sutured implantation, the motion of the native leaflets is typically hindered by the presence of the suture wrapped around the CT.

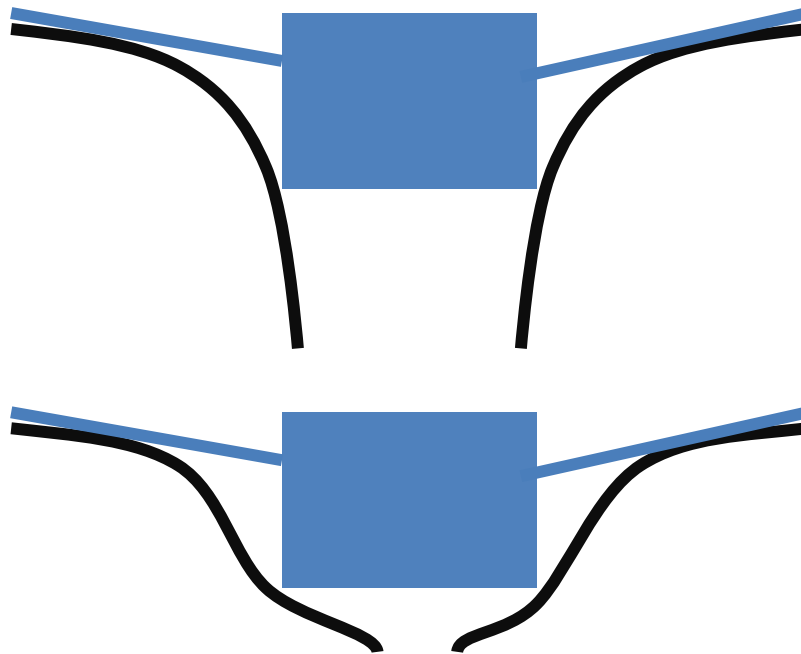


**Figure 43. An illustration of interference by the native mitral leaflets. The top image shows both valves during diastole and the bottom image shows the valves during systole. If the leaflets are long enough, they wrap around the top of the stent of the valve and begin to cover the orifice.**

Neither this study, nor any published literature, discusses the effects of a remodeling ventricle on the long term efficacy of percutaneous mitral valve implants. Functional MR results from a displacement of the PM that changes the CT tethering on the MV leaflets. This displacement can be due to either an increase in the sphericity of the left ventricle or a remodeling of the ventricular walls: This change in tethering causes poor coaptation of the MV leaflets and results in MR [39]. Surgical literature has shown that

repairing the MV in cases of functional MR can reduce the dimensions and sphericity of the left ventricle [39]. Assuming mitral replacement produces similar results to mitral replacement on the sphericity of the left ventricle, there is a potential for severe consequences of tethered TAMI implantation. If the reverse remodeling of the left ventricle sufficiently reduces the distance between the area of tether fixation and the mitral annulus, then the force of ventricular fixation of the prosthesis may be compromised. To date, there have been no published pre-clinical trials using a disease model such as this, so these effects have not been investigated. However, it has been shown by several research groups, that in chronic studies involving transapical mitral valves, there has been a moderate amount of tissue in growth of the valve on both the ventricular and atrial elements [25, 33]. Figures illustrating this tissue in growth can be seen in Figure 10 and Figure 11 in the Literature Review section. The fixating force of this tissue growth was not reported on in either of the publications, but should the tissue growth secure the valve into the native annulus, long term ventricular fixation would no longer be necessary. Thus, depending on the length of time in which cardiac anatomy would be remodeled, the prosthesis may still be securely fixated within the native annulus.

Functional MR also affects the size of the native mitral annulus, an increase in the septo-lateral distance is often seen in heart attack patients which results in poor leaflet coaptation. Similar to reduction in left ventricle dimension and sphericity, medical therapy can also reduce the dilation of the mitral annulus [39]. This has several consequences on implanted TAMI valves. Firstly, the decrease in septo-lateral distance of the annulus can place a larger amount of radial stress on the stent body of the valve,

which may have the potential of producing a fracture of the valve stent or may result in a crimping action of the valve stent that results in a malcoaptation of the prosthesis leaflets. Reduction of annular dilation on may also result in an increased interference from native mitral leaflets. This should not be a problem in TAMl implantation that hooks to the native leaflet tissue because the leaflets will be restrained; however, in tethered implantation, the leaflets are free to potentially impinge on the size of the prosthesis orifice.

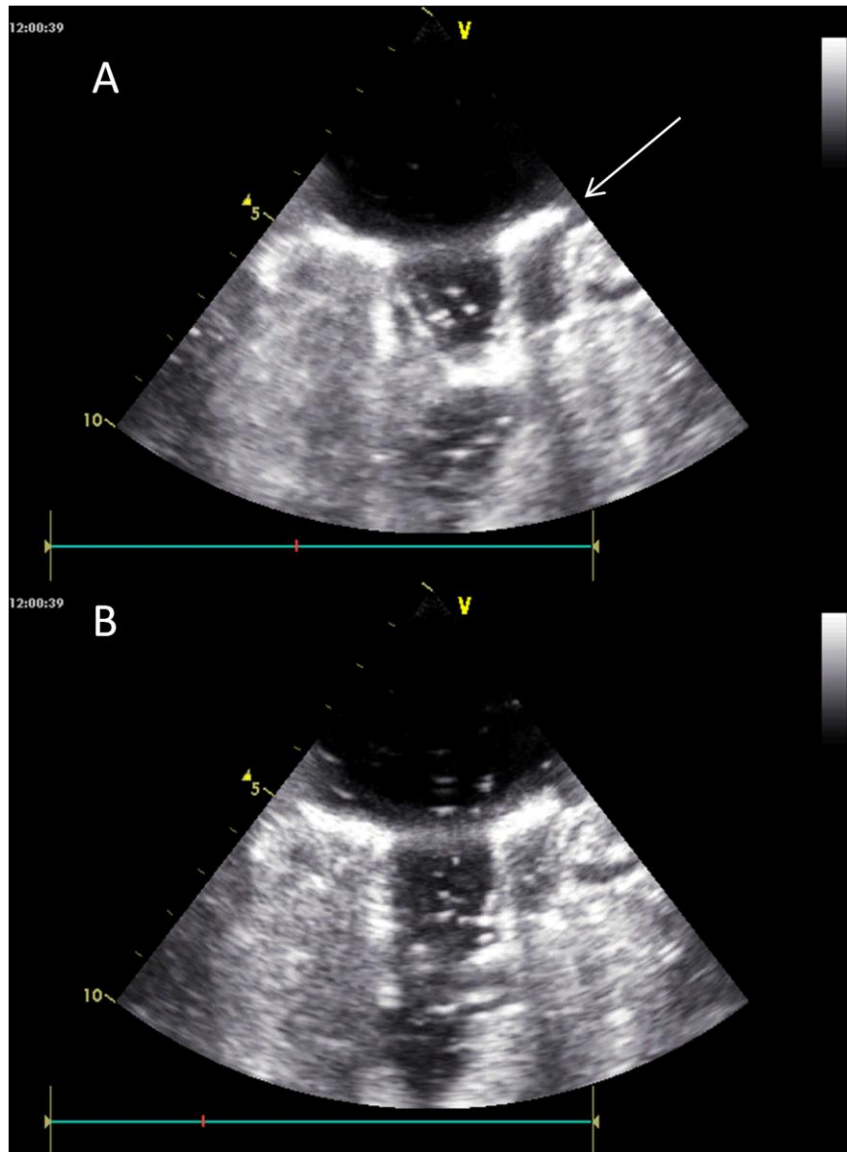


**Figure 44. Poor atrial fixation of the non-atrialized valve design implanted in the sutured fashion. (A) shows a gap forming between the atrial skirt of the valve and the atrial floor (pointed out by the white arrow) during high pressure systole and (B) shows that same gap disappearing during diastole.**

#### 4.5 Potential Future Work

Given the many things observed throughout the course of experimentation, there are several items that could be addressed as well as different areas of which to focus during future studies.

One important factor is the size of the mitral leaflets themselves: During sutured (hooked) implantation, the leaflets are restrained such that they do not interfere with normal prosthesis function; however, during tethered implantation, the leaflets are not restrained and larger leaflets may interfere with valve function. It would be an interesting way to optimize valve design based on fixation method by using a measurement of the mitral valve leaflet size and adjusting the stent height accordingly. The stent height would have to be optimally minimized to prevent LVOT obstruction, but large enough such that the native leaflets would not interfere with valve function.

It would also be interesting to artificially induce left ventricular and annular dilation before implantation in order to assess the efficacy of the TAMI valves in a disease model. Then study the long term effects by then artificially inducing remodeling of the left ventricle and annulus incrementally and observe the effects of valve efficiency.

## Chapter 5: Summary and Limitations

### 5.1 Aim 1 – Summary

The goal of aim 1 was to evaluate the leaflet kinematics and hemodynamics of the two TAMI valve designs. To accomplish this, a left heart simulator was used in conjunction with high speed imagery and particle image velocimetry techniques. The left heart simulator utilized a clear acrylic block in which the implanted mitral valve could be visualized. Pressure and flow wave forms, geometric orifice area, vorticity and velocity dynamics, and Reynolds shear stresses were evaluated for each valve design at a variety of conditions.

Both valve designs assessed showed adequate peak flows, average pressure gradients during diastole and filling dynamics during diastole. The peak flow during diastole at 60 bpm was between 250 and 300 mL/s and average pressure gradients were below 5 mmHg. At the beginning of diastole proper vortex ring formation occurred in both valves at each heart rate. The geometric orifice area for the atrialized valve design was notably less than that of the non-atrialized design; however, this is likely due to the atrialized nature of the leaflets and their slight impingement on the valve orifice.

The maximum velocities and RSS levels during diastole for both valve designs were slightly elevated: At 60 bpm, the maximum velocities were upwards of 1.3 m/s and RSS values were roughly 60 N/m<sup>2</sup> and above. Unfortunately there exists no control prosthesis for which to compare these values to. The elevated values can be contributed to the low viscosity of the working fluid (water) in conjunction with the

relatively small orifice area of these prostheses as compared to standard mitral bioprostheses. Although the valves showed elevated RSS values, they still fall within the safe range for red blood cell damage, but they may result in a slight amount of platelet activation. Further tests with a known control valve would be needed in order to be certain of any platelet activation that could potentially occur after implantation.

## 5.2 Aim 1 - Limitations

### 5.2.1 Idealized Left Ventricle

The left heart simulator utilizes an acrylic block housing the mitral and aortic valves as a simulation of the left ventricle. Obviously an acrylic block lacks many of the features of the left ventricle, including but not limited to: rigid housing, non-contractile, lack of trabeculations, and anatomically incorrect relationship of the mitral and aortic valves. The uniform and clear nature of the acrylic; however, is a perfect environment to accurately perform PIV and capture high speed imaging of the prosthetic valves. The acrylic block is an ideal environment to study the fluid mechanics in the immediate vicinity of the prosthesis.

### 5.2.2 Non Blood Analogue as Working Fluid

The working fluid used during PIV experiments was distilled water which has a different viscosity from blood. Oftentimes during in vitro experiments, a glycerine based viscosity and density matched solution is used as an analogue for blood. Results have shown that viscosity does not affect pressure drop and flow patterns and velocity profiles downstream do not differ between water and a blood analogue [40, 41]. In addition,

ISO standards for the testing of bioprosthetic heart valves indicate that it is not required to use a blood matched working fluid.

## 5.2 Aim 2 – Summary

The goal of aim 2 was to evaluate and understand the difference in mechanics between two different methods of ventricular fixation for transapical mitral valves. The two valve designs were implanted in a passively beating porcine heart and the paravalvular regurgitation was assessed.

Two flow probes were used to measure the total flow created by the diaphragm pump and the aortic flow rate to determine what amount of fluid was expelled by the pump but did not pass through the aortic valve. This volume was interpreted as the mitral regurgitant volume. Mitral regurgitant volume was divided by the total forward volume to end with a mitral regurgitant fraction or MRF. This value is a performance index with large values indicating a poorly performing valves and lower values indicating a valve that is performing well. In order to correct for the viscosity difference between the working fluid in the system (water) and the conditions in vivo, a viscosity correction was performed to obtain the final data.

Statistical testing of the final data resulted several significant comparisons: The atrialized valve was superior to the non-atrialized valve in sutured implantation and when both implant conditions were lumped together, the atrialized valve performed better than the non-atrialized valve. The difference between valve designs in the tethered implantation method was not statistically significant.

Both of the significant comparisons validated what was observed during experimentation. In sutured implantation, the large stent profile of the non-atrialized design resulted in a loosely seating atrial cuff which caused a large amount of paravalvular regurgitation. In contrast, the low ventricular stent height of the atrialized design produced a tight sealing of the atrial cuff against the floor of the left atrium. Due to its small ventricular stent height; however, the atrialized design was more susceptible to interference from the native valve leaflets. The interference typically only occurred during tethered implantation: When implanted in the sutured fashion, the native leaflets were inhibited from interfering by the anchoring sutures.

These observations show that the importance of the relationship between ventricular stent height and fixation method compared with native anatomy plays an important role in overall prosthesis function regardless of implantation method.

## 5.4 Aim 2 – Limitations

### 5.4.1 Paradoxical Ventricular Motion

The IVBHS functions by sending a pressurized slug of water into the left ventricle and out the aortic valve in order to simulate a beat of the heart. Due to the high pressure nature of this slug, the left ventricle expands during systole. In an *in vivo* environment, the left ventricle contracting during systole is what expels fluid out the aortic valve.

Because of this, the tissue sample in the IVBHS actually experiences a paradoxical motion during the cardiac cycle: It experiences the exact opposite of what occurs *in vivo* throughout the cardiac cycle.

This paradoxical motion should only have an effect on the tethered method of implantation, if it has any effect at all. In the sutured method, the valve is fixed relative to the native mitral tissue and it would not respond to any changes in the size or shape of the left ventricle.

#### 5.4.2 Porcine Model as Human Analogue

Many research studies use the ovine model for testing heart implants; however, the porcine heart has a greater similarity to the human heart in both size and mitral valve anatomy than the ovine heart. The porcine heart is very similar to the human heart with respect to the arrangement of mitral leaflets and distribution and number of chordae tendinae [42]. It was observed during experimentation, and noted in an in depth comparison of porcine and human cardiac anatomy, that the porcine heart contains a much thicker left ventricular wall. In addition to a thicker wall, the porcine left ventricle has contains larger papillary muscles and more course ventricular trabeculations [43]. The thick ventricular wall may be the most important distinction to note. While the resulting small ventricular cavity can prove difficult for imaging and attaining proper flow in some cases, it does not appear to affect the performance of the implanted bioprosthesis. Although some of the harvested hearts with especially small ventricular cavities proved difficult to prep due to the close proximity of the PM and CT to the hole created for the port: This would often result in either the PM or CT to be cut during heart prep and having to discard the heart.

#### 5.4.3 Replicating In Vivo Valve Implantation

Suturing the prosthesis into place using the native valve tissue is not an exact replica of a mechanical attachment to the same tissue; however, the process was replicated as

closely as possible. The attachment points selected for suturing were based off of those seen in the Tiara valve developed by Neovasc, Inc. It appears that the Tiara valve engages the native mitral leaflet using three hooking mechanisms at three different anatomical positions: The first and second positions occur at approximately the left and right fibrous trigones, while the third is centrally located on the posterior leaflet. As you can see in the section detailing valve implantation, these are the same anatomical positions as were chosen to be suture anchor points for the valves.

#### 5.4.4 Flow Probe Error

The clamp on flow meter being used was extremely susceptible to measurement error due to bubble formation in the system. Care was taken to bleed all air out of the system before use. This error presented itself as a relatively large inequality in the calculated values of total forward stroke and the total retrograde stroke. Any data in which there were distinct discrepancies between forward and retrograde stroke were thrown out.

## References

1. Tamburino, C., et al., *Percutaneous mitral valve repair with the MitraClip system: acute results from a real world setting*. European Heart Journal, 2010. **31**(11): p. 1382-1389.
2. Stanfield, C. and W. Germann, *Principles of Human Physiology*. Third ed2008: Pearson Education.
3. Rabbah, J.-P.M., et al., *Mechanics of Healthy and Functionally Diseased Mitral Valves: A Critical Review*. Journal of Biomechanical Engineering-Transactions of the Asme, 2013. **135**(2).
4. McCarthy, K.P., L. Ring, and B.S. Rana, *Anatomy of the mitral valve: understanding the mitral valve complex in mitral regurgitation*. European Journal of Echocardiography, 2010. **11**(10): p. I3-I9.
5. Silbiger, J.J., *Anatomy, mechanics, and pathophysiology of the mitral annulus*. American Heart Journal, 2012. **164**(2): p. 163-176.
6. Joudinaud, T.M., et al., *The papillary muscles as shock absorbers of the mitral valve complex. An experimental study*. European Journal of Cardio-Thoracic Surgery, 2007. **32**(1): p. 96-101.
7. Turi, Z.G., *Mitral valve disease*. Circulation, 2004. **109**(6): p. E38-E41.
8. Dasi, L.P., et al., *FLUID MECHANICS OF ARTIFICIAL HEART VALVES*. Clinical and Experimental Pharmacology and Physiology, 2009. **36**(2): p. 225-237.
9. Acker, M.A., et al., *Mitral-Valve Repair versus Replacement for Severe Ischemic Mitral Regurgitation*. New England Journal of Medicine, 2014. **370**(1): p. 23-32.

10. Go, A.S., et al., *Heart Disease and Stroke Statistics-2014 Update A Report From the American Heart Association*. Circulation, 2014. **129**(3): p. E28-E292.
11. Chiam, P.T.L. and C.E. Ruiz, *Percutaneous Transcatheter Mitral Valve Repair A Classification of the Technology*. Jacc-Cardiovascular Interventions, 2011. **4**(1): p. 1-13.
12. lung, B., et al., *Decision-making in elderly patients with severe aortic stenosis: why are so many denied surgery?* Eur Heart J, 2005. **26**(24): p. 2714-20.
13. Faxon, D.P., *Transcatheter Aortic Valve Implantation Coming of Age*. Circulation, 2011. **124**(17): p. E439-E440.
14. Thomas, M., et al., *Thirty-Day Results of the SAPIEN Aortic Bioprosthesis European Outcome (SOURCE) Registry A European Registry of Transcatheter Aortic Valve Implantation Using the Edwards SAPIEN Valve*. Circulation, 2010. **122**(1): p. 62-U130.
15. Yuan, Y.T., et al., *One-year results of transcatheter aortic valve implantation as an alternative treatment for severe aortic stenosis in high-risk patients*. Journal of the Chinese Medical Association, 2013. **76**(12): p. 698-702.
16. Wilbring, M., et al., *Transapical Transcatheter Valve-in-Valve Implantation for Deteriorated Mitral Valve Bioprostheses*. Annals of Thoracic Surgery, 2013. **95**(1): p. 111-118.
17. Cheung, A., et al., *5-Year Experience With Transcatheter Transapical Mitral Valve-in-Valve Implantation for Bioprosthetic Valve Dysfunction*. Journal of the American College of Cardiology, 2013. **61**(17): p. 1759-1766.

18. Wilbring, M., et al., *Pushing the limits-further evolutions of transcatheter valve procedures in the mitral position, including valve-in-valve, valve-in-ring, and valve-in-native-ring*. Journal of Thoracic and Cardiovascular Surgery, 2014. **147**(1): p. 210-219.
19. Himbert, D., et al., *Transseptal Implantation of a Transcatheter Heart Valve in a Mitral Annuloplasty Ring to Treat Mitral Repair Failure*. Circulation-Cardiovascular Interventions, 2011. **4**(4): p. 396-U164.
20. Hammerstingl, C., et al., *Percutaneous implantation of a 26 mm Edwards SAPIEN-XT aortic valve prosthesis in a degenerated 30 mm mitral annuloplasty ring*. European Heart Journal, 2013. **34**(23): p. 1748-1748.
21. Yun, K.L., et al., *Randomized trial comparing partial versus complete chordal-sparing mitral valve replacement: Effects on left ventricular volume and function*. Journal of Thoracic and Cardiovascular Surgery, 2002. **123**(4): p. 707-714.
22. Lutter, G., et al., *Mitral valved stent implantation*. European Journal of Cardio-Thoracic Surgery, 2010. **38**(3): p. 350-355.
23. Lutter, G., et al., *Off-pump transapical mitral valve replacement*. European Journal of Cardio-Thoracic Surgery, 2009. **36**(1): p. 124-128.
24. Banai, S., et al., *Transapical mitral implantation of the tiara bioprosthesis: pre-clinical results*. JACC Cardiovasc Interv, 2014. **7**(2): p. 154-62.
25. Attmann, T., et al., *Mitral valved stent implantation: an overview*. Minim Invasive Ther Allied Technol, 2011. **20**(2): p. 78-84.

26. Iino, K., et al., *Off-pump transapical mitral valve replacement: evaluation after one month*. European Journal of Cardio-Thoracic Surgery, 2012. **41**(3): p. 512-517.
27. Lozonschi, L., et al., *Transapical mitral valved stent implantation: a survival series in swine*. J Thorac Cardiovasc Surg, 2010. **140**(2): p. 422-426 e1.
28. Lozonschi, L. and G. Lutter, *Transcatheter mitral valve stent implantation*. Eurointervention, 2011. **6**(9): p. 1036-1036.
29. Lozonschi, L., et al., *Transapical mitral valved stent implantation*. Annals of Thoracic Surgery, 2008. **86**(3): p. 745-748.
30. Ma, L., et al., *Double-crowned valved stents for off-pump mitral valve replacement*. European Journal of Cardio-Thoracic Surgery, 2005. **28**(2): p. 194-198.
31. Boudjemline, Y., et al., *Steps toward the percutaneous replacement of atrioventricular valves - An experimental study*. Journal of the American College of Cardiology, 2005. **46**(2): p. 360-365.
32. Banai, S., et al., *Tiara: A Novel Catheter-Based Mitral Valve Bioprosthesis Initial Experiments and Short-Term Pre-Clinical Results*. Journal of the American College of Cardiology, 2012. **60**(15): p. 1430-1431.
33. Banai, S., et al., *TIARA - A Novel Catheter-Based Mitral Valve Bio-Prosthesis Short Term Pre-Clinical Results*. Journal of the American College of Cardiology, 2012. **60**(17): p. B33-B33.
34. Gillespie, M.J., et al., *Sutureless Mitral Valve Replacement: Initial Steps Toward a Percutaneous Procedure*. Annals of Thoracic Surgery, 2013. **96**(2): p. 670-674.

35. Ge, L., et al., *Characterization of hemodynamic forces induced by mechanical heart valves: Reynolds vs. viscous stresses*. *Ann Biomed Eng*, 2008. **36**(2): p. 276-97.
36. Yoganathan, A.P., Z. He, and S. Casey Jones, *Fluid mechanics of heart valves*. *Annu Rev Biomed Eng*, 2004. **6**: p. 331-62.
37. Pedrizzetti, G., F. Domenichini, and G. Tonti, *On the Left Ventricular Vortex Reversal after Mitral Valve Replacement*. *Ann Biomed Eng*, 2010. **38**(3): p. 769-773.
38. Bothe, W., D.C. Miller, and T. Doenst, *Sizing for Mitral Annuloplasty: Where Does Science Stop and Voodoo Begin?* *Annals of Thoracic Surgery*, 2013. **95**(4): p. 1475-1483.
39. Punnoose, L., et al., *Functional Mitral Regurgitation: Therapeutic Strategies for a Ventricular Disease*. *Journal of Cardiac Failure*, 2014. **20**(4): p. 252-267.
40. Muller-Hulsbeck, S., et al., *Flow patterns from metallic vascular endoprotheses: in vitro results*. *European Radiology*, 2001. **11**(5): p. 893-901.
41. Hanle, D.D., et al., *INVITRO FLOW DYNAMICS OF 4 PROSTHETIC AORTIC VALVES - A COMPARATIVE-ANALYSIS*. *Journal of Biomechanics*, 1989. **22**(6-7): p. 597-607.
42. Smerup, M., et al., *A long-term porcine model for evaluation of prosthetic heart valves*. *Heart Surgery Forum*, 2004. **7**(4): p. E259-E264.
43. Crick, S.J., et al., *Anatomy of the pig heart: comparisons with normal human cardiac structure*. *Journal of Anatomy*, 1998. **193**: p. 105-119.

Appendix I  
GOA Raw Data

**Table 5. Raw data for the geometric orifice area calculations of each valve design**

<b>Atrialized Valve</b>		
Cardiac Cycle	Area (pixels <sup>2</sup> )	GOA (cm <sup>2</sup> )
1	93742	2.51
1	92365	2.47
1	92075	2.47
1	90222	2.42
1	89463	2.40
1	90500	2.42
1	91222	2.44
1	94340	2.53
2	93776	2.51
2	92639	2.48
2	90571	2.43
2	89686	2.40
2	90379	2.42
2	90894	2.43
2	93030	2.49
2	93550	2.51
3	94851	2.54
3	93291	2.50
3	92027	2.46
3	90078	2.41
3	90098	2.41
3	90096	2.41
3	90939	2.44
3	93761	2.51

<b>Non-Atrialized Valve</b>		
Cardiac Cycle	Area (pixels <sup>2</sup> )	GOA (cm <sup>2</sup> )
1	93839	2.68
1	92928	2.65
1	89375	2.55
1	91052	2.60
1	95385	2.72
1	96267	2.75
1	96220	2.75
1	95596	2.73
2	93053	2.66
2	99703	2.85
2	93833	2.68
2	88339	2.52
2	92199	2.63
2	95431	2.72
2	96483	2.75
2	96161	2.74
3	96063	2.74
3	92662	2.64
3	88773	2.53
3	91873	2.62
3	94918	2.71
3	95976	2.74
3	94382	2.69
3	94759	2.70

## Appendix II

### Data from IVBHS Experimentation

## Heart 1

Native				
	Mean Systolic Stroke (mL)	St Dev	MAP	St Dev
Total	114.34	12.08	82.67	0.27
Aortic_Peak	31.12	0.32	84.97	0.52
Stroke Volume	27.88	0.08		
Mean Beatwise Systolic Regurg	83.21	12.07		
MRF	0.73	0.13		
Leakage Fraction (Aortic/Total)	0.27	0.03		
Cardiac Output (L/min)	1.87	0.02		
Non-Atrialized: Tether				
	Mean Systolic Stroke (mL)	St Dev	MAP	St Dev
Total	127.45	4.65	72.36	0.13
Aortic_Peak	43.58	0.78	84.43	0.81
Stroke Volume	36.51	0.08		
Mean Beatwise Systolic Regurg	83.87	4.58		
MRF	0.66	0.04		
Leakage Fraction (Aortic/Total)	0.34	0.01		
Cardiac Output (L/min)	2.61	0.05		
Non-Atrialized: Sutured				
	Mean Systolic Stroke (mL)	St Dev	MAP	St Dev
Total	181.11	10.56	91.39	0.83
Aortic_Peak	47.12	1.51	89.98	1.26
Stroke Volume	34.16	0.02		
Mean Beatwise Systolic Regurg	133.98	10.45		
MRF	0.74	0.07		
Leakage Fraction (Aortic/Total)	0.26	0.02		
Cardiac Output (L/min)	2.83	0.09		
Atrialized: Tether				
	Mean Systolic Stroke (mL)	St Dev	MAP	St Dev
Total	141.54	13.56	92.46	1.55
Aortic_Peak	36.72	0.80	84.24	0.87
Stroke Volume	27.83	0.05		
Mean Beatwise Systolic Regurg	104.82	13.53		
MRF	0.74	0.12		
Leakage Fraction (Aortic/Total)	0.26	0.03		
Cardiac Output (L/min)	2.20	0.05		
Atrialized: Sutured				
	Mean Systolic Stroke (mL)	St Dev	MAP	St Dev
Total	162.05	1.59	85.10	0.25
Aortic_Peak	41.73	0.34	84.90	0.15
Stroke Volume	37.13	0.03		
Mean Beatwise Systolic Regurg	120.32	1.56		
MRF	0.74	0.01		
Leakage Fraction (Aortic/Total)	0.26	0.00		
Cardiac Output (L/min)	2.50	0.02		

**Figure 45 Raw data for Heart 1**

## Heart 2

Native				
	Mean Systolic Stroke (mL)	St Dev	MAP	St Dev
Total	111.10	1.21	83.86	0.81
Aortic_Peak	28.78	2.27	95.15	2.11
Stroke Volume	22.13	0.05		
Mean Beatwise Systolic Regurg	82.31	1.92		
MRF	0.74	0.02		
Leakage Fraction (Aortic/Total)	0.26	0.02		
Cardiac Output (L/min)	1.73	0.14		
Non-Atrialized: Tether				
	Mean Systolic Stroke (mL)	St Dev	MAP	St Dev
Total	132.88	5.30	102.21	3.82
Aortic_Peak	41.73	19.88	103.58	4.32
Stroke Volume	43.56	0.04		
Mean Beatwise Systolic Regurg	91.15	19.16		
MRF	0.69	0.15		
Leakage Fraction (Aortic/Total)	0.31	0.15		
Cardiac Output (L/min)	2.50	1.19		
Non-Atrialized: Sutured				
	Mean Systolic Stroke (mL)	St Dev	MAP	St Dev
Total	137.07	1.11	99.58	0.10
Aortic_Peak	39.74	0.27	96.39	0.21
Stroke Volume	36.13	0.02		
Mean Beatwise Systolic Regurg	97.33	1.08		
MRF	0.71	0.01		
Leakage Fraction (Aortic/Total)	0.29	0.00		
Cardiac Output (L/min)	2.38	0.02		
Atrialized: Tether				
	Mean Systolic Stroke (mL)	St Dev	MAP	St Dev
Total	116.34	2.11	97.69	0.24
Aortic_Peak	39.89	0.81	95.43	0.54
Stroke Volume	37.12	0.08		
Mean Beatwise Systolic Regurg	76.45	1.95		
MRF	0.66	0.02		
Leakage Fraction (Aortic/Total)	0.34	0.01		
Cardiac Output (L/min)	2.39	0.05		
Atrialized: Sutured				
	Mean Systolic Stroke (mL)	St Dev	MAP	St Dev
Total	75.86	0.29	99.56	0.12
Aortic_Peak	41.46	0.32	98.87	0.07
Stroke Volume	37.06	0.01		
Mean Beatwise Systolic Regurg	34.40	0.14		
MRF	0.45	0.00		
Leakage Fraction (Aortic/Total)	0.55	0.00		
Cardiac Output (L/min)	2.49	0.02		

**Figure 46. Raw data for Heart 2**

### Heart 3

Native				
	Mean Systolic Stroke (mL)	St Dev	MAP	St Dev
Total	118.83	3.07	100.68	0.08
Aortic_Peak	58.24	0.34	101.31	0.14
Stroke Volume	56.06	0.00		
Mean Beatwise Systolic Regurg	60.58	3.05		
MRF	0.51	0.03		
Leakage Fraction (Aortic/Total)	0.49	0.01		
Cardiac Output (L/min)	3.49	0.02		
Non-Atrialized: Tether				
	Mean Systolic Stroke (mL)	St Dev	MAP	St Dev
Total	78.77	0.91	112.98	0.17
Aortic_Peak	10.05	0.15	104.48	1.03
Stroke Volume	2.23	0.03		
Mean Beatwise Systolic Regurg	68.73	0.90		
MRF	0.87	0.02		
Leakage Fraction (Aortic/Total)	0.13	0.00		
Cardiac Output (L/min)	0.60	0.01		
Non-Atrialized: Sutured				
	Mean Systolic Stroke (mL)	St Dev	MAP	St Dev
Total	193.87	2.80	96.28	0.13
Aortic_Peak	58.70	0.47	97.47	0.21
Stroke Volume	55.00	0.06		
Mean Beatwise Systolic Regurg	135.17	2.76		
MRF	0.70	0.02		
Leakage Fraction (Aortic/Total)	0.30	0.01		
Cardiac Output (L/min)	3.52	0.03		
Atrialized: Tether				
	Mean Systolic Stroke (mL)	St Dev	MAP	St Dev
Total	130.63	1.33	96.65	0.08
Aortic_Peak	58.60	0.58	97.39	0.10
Stroke Volume	56.57	0.02		
Mean Beatwise Systolic Regurg	72.03	1.19		
MRF	0.55	0.01		
Leakage Fraction (Aortic/Total)	0.45	0.01		
Cardiac Output (L/min)	3.52	0.03		

**Figure 47. Raw data for Heart 3**

## Heart 4

Native				
	Mean Systolic Stroke (mL)	St Dev	MAP	St Dev
Total	126.60	2.21	96.77	3.33
Aortic_Peak	19.29	0.33	79.13	0.22
Stroke Volume	15.07	0.04		
Mean Beatwise Systolic Regurg	107.31	2.18		
MRF	0.85	0.02		
Leakage Fraction (Aortic/Total)	0.15	0.00		
Cardiac Output (L/min)	1.16	0.02		
Non-Atrialized: Tether				
	Mean Systolic Stroke (mL)	St Dev	MAP	St Dev
Total	145.99	1.21	-14.35	0.00
Aortic_Peak	45.54	0.34	-14.35	0.00
Stroke Volume	42.82	0.02		
Mean Beatwise Systolic Regurg	100.45	1.17		
MRF	0.69	0.01		
Leakage Fraction (Aortic/Total)	0.31	0.00		
Cardiac Output (L/min)	2.73	0.02		
Non-Atrialized: Sutured				
	Mean Systolic Stroke (mL)	St Dev	MAP	St Dev
Total	108.63	0.99	98.90	0.12
Aortic_Peak	47.03	0.56	98.26	0.11
Stroke Volume	40.80	0.01		
Mean Beatwise Systolic Regurg	61.60	0.82		
MRF	0.57	0.01		
Leakage Fraction (Aortic/Total)	0.43	0.01		
Cardiac Output (L/min)	2.82	0.03		
Atrialized: Tether				
	Mean Systolic Stroke (mL)	St Dev	MAP	St Dev
Total	119.51	1.19	93.53	2.95
Aortic_Peak	45.82	6.43	99.25	2.50
Stroke Volume	47.18	0.05		
Mean Beatwise Systolic Regurg	73.69	6.32		
MRF	0.62	0.05		
Leakage Fraction (Aortic/Total)	0.38	0.05		
Cardiac Output (L/min)	2.75	0.39		
Atrialized: Sutured				
	Mean Systolic Stroke (mL)	St Dev	MAP	St Dev
Total	98.12	0.72	95.25	0.26
Aortic_Peak	44.97	0.51	95.86	0.19
Stroke Volume	41.03	0.02		
Mean Beatwise Systolic Regurg	53.15	0.51		
MRF	0.54	0.01		
Leakage Fraction (Aortic/Total)	0.46	0.01		
Cardiac Output (L/min)	2.70	0.03		

**Figure 48. Raw data for Heart 4**

## Heart 5

Native					
	Mean Systolic Stroke (mL)	St Dev	MAP	St Dev	
Total	114.52	2.08	85.73	0.64	
Aortic_Peak	53.60	0.91	88.13	1.16	
Stroke Volume	49.88	0.02			
Mean Beatwise Systolic Regurg	60.93	1.87			
MRF	0.53	0.02			
Leakage Fraction (Aortic/Total)	0.47	0.01			
Cardiac Output (L/min)	3.22	0.05			
Non-Atrialized: Tether					
	Mean Systolic Stroke (mL)	St Dev	MAP	St Dev	
Total	145.99	1.21	-14.35	0.00	
Aortic_Peak	45.54	0.34	-14.35	0.00	
Stroke Volume	42.82	0.02			
Mean Beatwise Systolic Regurg	100.45	1.17			
MRF	0.69	0.01			
Leakage Fraction (Aortic/Total)	0.31	0.00			
Cardiac Output (L/min)	2.73	0.02			
Non-Atrialized: Sutured					
	Mean Systolic Stroke (mL)	St Dev	MAP	St Dev	
Total	126.20	2.09	98.19	0.09	
Aortic_Peak	52.02	0.39	98.19	0.10	
Stroke Volume	49.13	0.01			
Mean Beatwise Systolic Regurg	74.18	2.05			
MRF	0.59	0.02			
Leakage Fraction (Aortic/Total)	0.41	0.01			
Cardiac Output (L/min)	3.12	0.02			
Atrialized: Tether					
	Mean Systolic Stroke (mL)	St Dev	MAP	St Dev	
Total	154.56	4.65	94.52	1.81	
Aortic_Peak	47.55	2.77	96.06	2.09	
Stroke Volume	39.41	0.11			
Mean Beatwise Systolic Regurg	107.01	3.74			
MRF	0.69	0.03			
Leakage Fraction (Aortic/Total)	0.31	0.02			
Cardiac Output (L/min)	2.85	0.17			
Atrialized: Sutured					
	Mean Systolic Stroke (mL)	St Dev	MAP	St Dev	
Total	95.35	0.80	90.54	0.09	
Aortic_Peak	51.25	0.58	90.66	0.10	
Stroke Volume	48.30	0.03			
Mean Beatwise Systolic Regurg	44.10	0.55			
MRF	0.46	0.01			
Leakage Fraction (Aortic/Total)	0.54	0.01			
Cardiac Output (L/min)	3.08	0.03			

**Figure 49. Raw data for Heart 5**

## Heart 6

Native				
	Mean Systolic Stroke (mL)	St Dev	MAP	St Dev
Total	134.29	2.54	111.65	0.42
Aortic_Peak	54.48	0.31	105.17	0.89
Stroke Volume	50.04	0.02		
Mean Beatwise Systolic Regurg	79.82	2.52		
MRF	0.59	0.02		
Leakage Fraction (Aortic/Total)	0.41	0.01		
Cardiac Output (L/min)	3.27	0.02		
Non-Atrialized: Tether				
	Mean Systolic Stroke (mL)	St Dev	MAP	St Dev
Total	123.66	2.62	101.61	0.81
Aortic_Peak	53.54	0.34	101.80	0.36
Stroke Volume	48.46	0.07		
Mean Beatwise Systolic Regurg	70.12	2.60		
MRF	0.57	0.02		
Leakage Fraction (Aortic/Total)	0.43	0.01		
Cardiac Output (L/min)	3.21	0.02		
Non-Atrialized: Sutured				
	Mean Systolic Stroke (mL)	St Dev	MAP	St Dev
Total	137.20	3.62	102.05	0.14
Aortic_Peak	54.28	0.38	98.88	0.15
Stroke Volume	48.43	0.08		
Mean Beatwise Systolic Regurg	82.91	3.60		
MRF	0.60	0.03		
Leakage Fraction (Aortic/Total)	0.40	0.01		
Cardiac Output (L/min)	3.26	0.02		
Atrialized: Tether				
	Mean Systolic Stroke (mL)	St Dev	MAP	St Dev
Total	113.71	6.88	106.40	0.18
Aortic_Peak	56.57	0.63	105.47	0.19
Stroke Volume	51.65	0.03		
Mean Beatwise Systolic Regurg	57.14	6.86		
MRF	0.50	0.07		
Leakage Fraction (Aortic/Total)	0.50	0.03		
Cardiac Output (L/min)	3.39	0.04		
Atrialized: Sutured				
	Mean Systolic Stroke (mL)	St Dev	MAP	St Dev
Total	132.26	3.37	96.81	0.19
Aortic_Peak	56.22	0.34	97.23	0.06
Stroke Volume	50.56	0.05		
Mean Beatwise Systolic Regurg	76.04	3.35		
MRF	0.57	0.03		
Leakage Fraction (Aortic/Total)	0.43	0.01		
Cardiac Output (L/min)	3.37	0.02		

**Figure 50. Raw data for Heart 6**

## Heart 7

Native					
	Mean Systolic Stroke (mL)	St Dev	MAP	St Dev	
Total	79.49	0.31	100.71	0.31	
Aortic_Peak	56.79	0.45	100.02	0.31	
Stroke Volume	52.80	0.08			
Mean Beatwise Systolic Regurg	22.70	0.32			
MRF	0.29	0.00			
Leakage Fraction (Aortic/Total)	0.71	0.01			
Cardiac Output (L/min)	3.41	0.03			
Non-Atrialized: Tether					
	Mean Systolic Stroke (mL)	St Dev	MAP	St Dev	
Total	94.88	0.85	116.18	0.63	
Aortic_Peak	54.30	0.74	109.37	0.75	
Stroke Volume	51.48	0.02			
Mean Beatwise Systolic Regurg	40.57	0.41			
MRF	0.43	0.01			
Leakage Fraction (Aortic/Total)	0.57	0.01			
Cardiac Output (L/min)	3.26	0.04			
Non-Atrialized: Sutured					
	Mean Systolic Stroke (mL)	St Dev	MAP	St Dev	
Total	133.58	2.08	101.26	0.30	
Aortic_Peak	56.52	0.34	100.95	0.18	
Stroke Volume	51.35	0.01			
Mean Beatwise Systolic Regurg	77.07	2.05			
MRF	0.58	0.02			
Leakage Fraction (Aortic/Total)	0.42	0.01			
Cardiac Output (L/min)	3.39	0.02			
Atrialized: Tether					
	Mean Systolic Stroke (mL)	St Dev	MAP	St Dev	
Total	84.82	1.79	103.91	0.10	
Aortic_Peak	55.78	0.35	102.43	0.19	
Stroke Volume	51.31	0.04			
Mean Beatwise Systolic Regurg	29.05	1.75			
MRF	0.34	0.02			
Leakage Fraction (Aortic/Total)	0.66	0.01			
Cardiac Output (L/min)	3.35	0.02			
Atrialized: Sutured					
	Mean Systolic Stroke (mL)	St Dev	MAP	St Dev	
Total	87.68	0.73	102.98	0.06	
Aortic_Peak	55.26	0.34	102.51	0.12	
Stroke Volume	52.17	0.03			
Mean Beatwise Systolic Regurg	32.42	0.64			
MRF	0.37	0.01			
Leakage Fraction (Aortic/Total)	0.63	0.01			
Cardiac Output (L/min)	3.32	0.02			

**Figure 51. Raw data for Heart 7.**

## Appendix III

### Matlab Code for Turbulence Analysis

## FunctionBJ

```
%Goes through the specified number of B files, where B number format is:  
%B00001. Calls VelOut function, which loadvecs all files within B file...  
%B00001_01, etc. Then that function outputs a average vector fileish.
```

```
%Specify how many B Numbers to go through:  
numBN=261;
```

```
%Go through each B number:  
for BN=1:1:numBN
```

```
    %Converts number to string with 0s in front with a total of numPlaces  
    %places
```

```
    %Initialize numStr:  
    BNS='B00000';
```

```
    %Convert num to string:  
    ns=mat2str(BN);
```

```
    %Get the number of characters in the number  
    numChar=size(ns,2);
```

```
    BNS(end-numChar+1:end)=ns;
```

```
    VelOut(BNS,BN)  
end
```

## Function VelOut

```
function VelOut(BNumString,BNum)

% This program will calculate the mean of Vx' and Vy' and print a dat file
% from which contours plot can be drawn easily

v=loadvec ([BNumString '*.vc7']); %reading the value

[p1,q1]=size(v);

image = q1;

%% Reading the Vx and Vy data and making mean & Standard deviation of velocity

for q=1:1:128 % (changed 256-128) reading the data of every point and making mean
and std
    for p=1:1:128 % changed 124-128
        for i=1:1:image
            velox(i)=v(1,i).vx(q,p);
            veloy(i)=v(1,i).vy(q,p);
        end;
        meanx(q,p)=mean(velox);
        meany(q,p)=mean(veloy);

        stdx(q,p)=std(velox);
        stdy(q,p)=std(veloy);
    end;
end;

preoutlierx=0;
prevelox=0;
preoutliery=0;
preveloy=0;
presuminvelox1=0;
presuminveloy1=0;
presuminveloxy=0;
%% Data Truncation
for i=1:1:image
    velox=v(1,i).vx(:,,:);
    outlierx=abs(velox-meanx) > 3*stdx;
    outlierx_sum=outlierx+preoutlierx;% getting a matix where the outliers are
    preoutlierx=outlierx_sum;% Summing them at all images
```

```

fvelox=velox.*~outliery; % negelecting the outliers from the sums
fvelox_sum=fvelox+prevelox;
prevelox=fvelox_sum;
v2(1,i).velox(:,:)=fvelox(:,:);

veloy=v(1,i).vy(:,:);
outliery=abs(veloy-meany) > 3*stdy;
outliery_sum=outliery+preoutliery;% getting a matix where the outliers are
preoutliery=outliery_sum;% Summing them at all images

fveloy=veloy.*~outliery; % negelecting the outliers from the sums
fveloy_sum=fveloy+preveloy;
preveloy=fveloy_sum;
v2(1,i).veloy(:,:)=fveloy(:,:);
end;

meanvelox=fvelox_sum./(image-outliery_sum); % new mean after removing outliers
meanveloy=fveloy_sum./(image-outliery_sum);

%% Subtracting mean velocity from instantenous velocity square them and
%% again making them mean
for i=1:1:image
    veloxx=v2(1,i).velox(:,:);
    invelox=(veloxx-meanvelox);
    invelox1=invelox.*invelox;
    suminvelox1=presuminvelox1+invelox1;
    presuminvelox1=suminvelox1;

    veloyy=v2(1,i).veloy(:,:);
    inveloy=(veloyy-meanveloy);
    inveloy1=inveloy.*inveloy;
    suminveloy1=presuminveloy1+inveloy1;
    presuminveloy1=suminveloy1;

    inveloxy=invelox.*inveloy; % for Vx'Vy'
    suminveloxy=presuminveloxy+inveloxy;
    presuminveloxy=suminveloxy;
end;

%% Making square root
secmeanx=suminvelox1./(image-outliery_sum);
veldashx=sqrt(secmeanx);

secmeany=suminveloy1./(image-outliery_sum);
veldashy=sqrt(secmeany);

```

```

secmeanxy=suminveloxy./(image-(outliery_sum+outliery_sum)); % for Vx'Vy'

%% taking x position and y position which will be used to print the file
xpos=v(1,1).x(1,:);
ypos=v(1,1).y(1,:);

[mx nx]=size(xpos);
[my ny]=size(ypos);

%% Printing file
textfilename=['VelOut_Output' '_B' mat2str(BNum) '.dat']; % Writing the file and storing
data in it
fid=fopen(textfilename, 'wt');

    fprintf (fid,...
        'VARIABLES = "X position","Y
position","Vx","Vy","Vxdash","Vydash","VxVydash"\n'...
        ); % writing the column header
    fprintf (fid,'ZONE T="Frame 01", I= %02d, J=%02d\n',nx,ny);
    for p=128:-1:1; %changed!
        for q=1:1:128; %changed!
            fprintf(fid,'%8.4f\t%8.4f\t%8.4e\t%8.4e\t%8.4e\t%8.4e\t%8.4e\t\n',...
                xpos(1,q), ypos(1,p),meanvelox(q,p),meanveloy(q,p),...
                veldashx(q,p),veldashy(q,p),secmeanxy(q,p));
        end;
    end;
fclose (fid);

```

## LIST OF ABBREVIATIONS

LVOT – Left Ventricular Outflow Tract

TAMI – Trans Apical Mitral Implantation

TAVI – Transcatheter Aortic Valve Implantation

PVL – Paravalvular Leakage

PVR – Paravalvular Regurgitation

MR – Mitral Regurgitation

MAP – Mean Arterial Pressure

PIV – Particle Image Velocimetry

MV – Mitral Valve

CT – Chordae Tendinae

PM – Papillary Muscle

SAM – Systolic Anterior Motion

LF – Leakage Fraction

GOA – Geometric Orifice Area

mmHg – Millimeters of Mercury

mL – Milliliters

RSS – Reynolds Shear Stress

RBCs – Red Blood Cells